REMARKS

This amendment responds to the office action mailed on May 10, 2002. In the office action the Examiner:

- rejected claims 32, 38, 44, 47, and 51-65 under 35 U.S.C. 112, second paragraph, as indefinite;
- rejected claims 1, 3-5, 28, 29, 33, 34, 54, 56, 58, and 60-65 under 35 U.S.C. 103(a) as being unpatentable over Char et al. (5,157,466) in view of Ishimaru et al. (5,883,051);
- rejected claims 2, 30, 31, and 52 under 35 U.S.C. 103(a) as being unpatentable over Char et al. (5,157,466) in view of Ishimaru et al. (5,883,051) and further in view of Shnirman et al. (Physical Review B 57, p. 15400, 1998);
- rejected claims 6, 8-10, 35, 39, 40, 41, 53, 55, 57, and 59 under 35 U.S.C. 103(a) as being unpatentable over Char et al. in view of Ishimaru et al. (5,883,051) and further in view of Baechtold et al. (3,953,749); and
- rejected claims 7, 11, 12-18, 36, 37, 42, 43, 45, 46, and 48-50 under 35 U.S.C. 103(a) as being unpatentable over Char et al. in view of Ishimaru et al. (5,883,051), Baechtold et al. (3,953,749), and further in view of Shnirman et al. (Physical Review B 57, p. 15400, 1998);

After entry of this amendment, the pending claims are claims 1-18 and 28-65.

Rejection of Claims Under 35 U.S.C. § 112, Second Paragraph

The Examiner has rejected claims 32, 38, 44, 47, and 51-65 under 35 U.S.C. 112, second paragraph, for four reasons. First, the Examiner contends that the meaning of the parity key, as recited in claims 32, 38, 44, 47, 51, and 61, is not clear. Second, the Examiner contends that is not clear where the clockwise and counterclockwise supercurrents recited in claims 52-55 are circulating. Third, the Examiner contends that the meaning of the term "twice degenerate states", as recited in claims 56-59, is not clear. Fourth, the Examiner contends that the tunneling between degenerate states recited in claims 60 and 64 is not clear. Applicant addresses each rejection in turn.

PARITY KEYS

Claims 32, 38, 44, 47, and 51-65 have been rejected under 35 U.S.C. 112, second paragraph for reciting the term "parity key." Applicant respectfully traverses

the rejection. To answer the question posed by the Examiner in the May 10, 2002 office action, the term "parity key" does not mean the "parity check" that is commonly found in computer science arts. On page 13 of Applicant's March 1, 2002 response to the October 1, 2001 office action, Applicant indicated that a parity key is a special form of a single-electron transistor (SET). In the October 1, 2001 office action, the Examiner rejected claim 15 under 35 U.S.C. 112, first paragraph, on the contention that the structure of a SET is not known. To respond to this rejection, Applicant discussed the fabrication, design, and function of SETs on pages 11 and 12 of the March 1, 2002 response. In the May 10, 2002 office action, the term SET was no longer rejected under 35 U.S.C. 112, first paragraph.

As is well known in the art, a parity key is a superconducting SET. The parity key only passes Cooper pairs (pairs of electrons), and only at certain gate voltages. The reference GL, which was submitted in the March 21, 2002 information disclosure statement, describes the physical properties of parity keys. (P. Joyez et al., "Observation of Parity-Induced Suppression of Josephson Tunneling in the Superconducting Single Electron Transistor", Physical Review Letters, Vol. 72:15, 2458-2461, April 11, 1994). Reference GL was incorporated by reference on page 15, line 17, of the specification.

The specification clearly illustrates the structure, function and use of parity keys. For example, page 14, lines 23-24, of the specification states that element 640 of Fig. 6 is a parity key or a SET. Inspection of Figure 6 shows that the structure of a parity key is clearly illustrated. Furthermore, to show that the term "parity key" is well known in the art, Applicant provides the reference Blais and Zagoskin, arXiv:quant-ph/9905043 v.2 (April 7, 2000) as Appendix C. In the last paragraph of column 1, the reference defines a parity key as a superconducting SET. Furthermore, Fig. 1a of the reference shows five parity keys, each designated "PK". The reference further refers to two other references for additional disclosure on the physical properties of SETs. One of the two references cited is reference GL submitted in the March 21, 2002 information disclosure statement. The other reference cited is Matveev *et al.*, "Parity-induced suppression of the Coulomb blockade of Josephson tunneling," Phys. Rev. Lett. 70, 2940 (1993). If desired, the Applicant can provide additional references to refer to "parity keys" in order to establish that the term "parity key" as recited in claims 32, 38, 44, 47, and 51-65 particularly point out and distinctly claim Applicant's invention.

CLOCKWISE AND COUNTERCLOCKWISE SUPERCURRENTS

The Examiner has rejected claims 52-55 on the contention that these claims recite a clockwise or counterclockwise circulating supercurrent without specifying where these supercurrents are circulating. Applicant has amended claims 52-55 to recite that supercurrents are circulating in a plane in the vicinity of the clean Josephson junction. Support for this amendment is found on page 6, lines 25-29, and page 9, lines 8-12, of the specification as well as Figure 1A. In particular Fig. 1A shows a circle with arrows to indicate the path of one such supercurrent. In some embodiments of the invention that are encompassed by claims 52-55, the island or the bank is made of a d-wave superconductor and the clockwise and/or counter clockwise supercurrent flows in the ab-plane of the d-wave material. See specification, page 6, lines 21-28. The orientation of the ab plane, in accordance with some embodiments of the invention, is shown in Figures 1B and 1C.

TWICE DEGENERATE STATES

The Examiner contends that the meaning of the term "twice degenerate states," as recited in claims 56-59, is not clear. Applicant traverses the rejection. Claims 56-59 recite a quantum state of a qubit. These claims further recite that this quantum state is twice degenerate. The twice degenerate state recited in claims 56-59 refers to a qubit having two stable energy states each having the same energy. With reference to Fig 1A, page 9, lines 8-12 states:

> Two degenerate states having the ground state energy and definite magnetic moment correspond to minimal supercurrents circulating through Josephson junction 130 in clockwise and counterclockwise senses, in a preferred plane of the crystal structures of bank 110 and/or island 120.

Thus, in the embodiment illustrated in Fig. 1A, one of the degenerate states refers to the supercurrent flowing in the clockwise direction and the other degenerate state refers to the supercurrent flowing in the counterclockwise direction in a preferred plane of the island or the bank.

Further clarity on the recitation of the term "doubly degenerate is found on page 6, lines 21-28, of the specification:

With a d-wave superconductor on at least one side of the Josephson junction, the Josephson junction has non-zero ground state supercurrent in the vicinity of the junction. This ground state supercurrent is either clockwise or counterclockwise in the preferred (so called ab-) plane of the d-wave superconductor. The ground state supercurrent in the vicinity of each Josephson junction is thus doubly degenerate and provides the basis for a quantum coherer or a qubit for quantum computing in accordance with an embodiment of the invention.

This passage clearly shows that claims 56-59 are particularly pointing out and distinctly claiming the subject matter that Applicant regards as his invention.

The concept of degenerate energy states is well known in the field of quantum mechanics. Degenerate level is defined in *Dictionary of Physics*, Longman, Singapore, 1958 as "An energy level of a quantum mechanical system that corresponds to more than one quantum state." Applicant provides the reference as Appendix D. A twice-degenerate state illustrated as a potential energy diagram is provided in Figure 1.

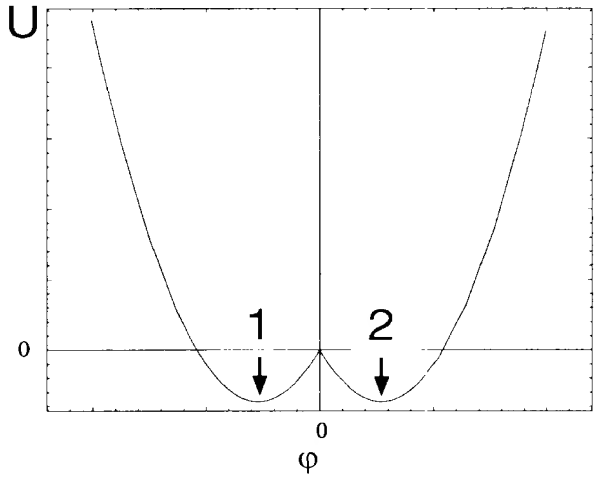

FIGURE 1

In Figure 1, "1" and "2" describe two potential energy wells in a potential energy diagram for the qubit recited in claims 56-59. As illustrated, states "1" and "2" are degenerate because the energies of the two states are the same. State "1" may represent the clockwise supercurrent and state "2" may represent the counterclockwise supercurrent that circulates across the Josephson junction as illustrated in Fig. 1A.

TUNNELING BETWEEN DEGENERATE STATES

The Examiner has rejected claims 60 and 64 because they recite the phrase "tunneling" within the limitation "quantum tunneling between the first ground state and the second ground state of the supercurrent associated with each Josephson junction." The first ground state and the second ground state of the system recited in claims 60 and 64 correlate with circulation directions of the supercurrent. For example, using Figure 1 above as a reference, the energy states "1" and "2" could represent the first ground state and the second ground state of the system. The term "quantum tunneling" refers to the phenomena in which the system shifts from state "1" to state "2" or vice versa.

To establish that the term "quantum tunneling" is an art recognized expression, Applicant provides the reference Mooij *et al.*, 1999, "Josephson Persistent Current Qubit," Science 285, pp. 1036-1039 as Appendix E. Mooij *et al.* is reference IK submitted in the March 21, 2002 information disclosure statement. On page 1037, column 2, of the reference, it is states that "The barrier of quantum tunneling between the states depends strongly on the value of α." Without elaborating on the meaning of α within the context of the Mooij *et al.* reference, the reference establishes that the phrase "quantum tunneling" is a well-defined art accepted term. Accordingly, the Examiner's rejection of the term "tunneling" as recited in claims 60 and 64 is improper and the Applicant respectfully requests that the rejection be withdrawn.

DOUBLE PATENTING REJECTION

The Examiner provisionally rejected claims 1-18 and claims 28-65 under the judicially created doctrine of obviousness-type double patenting as being unpatentable over claims 1-27 of copending application 09/855,817. Applicant traverses the rejection. The rejection is improper as a matter of law. The third sentence of 35 U.S.C. 121 states:

> A patent issuing on an application with respect to which a requirement for restriction under this section has been made, or on an application filed as a result of such a requirement, shall not be used as a reference either in the Patent and Trademark Office or in the courts against a divisional application or against the original application or any patent issued on either of them, if the application is filed before the issuance of the patent on the other application.

Copending application 09/855,817 is a divisional application of the present application. On February 23, 2001, the Examiner imposed a restriction requirement between Group I (claims 1-18 drawn to a quantum computing structure) and Group II (claims 19-27 drawn to a process). On March 16, 2001, Applicant elected without traverse to have the invention of Group I (claims 1-18) examined. All presently pending claims are drawn to a quantum computing structure and are thus properly classified as Group I claims in accordance with the February 23, 2001 restriction requirement.

On May 14, 2001, divisional application 09/855,817 was filed. The preliminary amendment, filed with application 09/855,817, cancelled claims 1-18. Thus, all that was pending in the divisional application was the claims of Group II as defined in the February 23, 2001 restriction requirement (claims 19-27). Although subsequent prosecution in the 09/855,817 application has resulted in additional pending claims in that application, each of the new pending claims is properly classified as a Group II claim in accordance with the February 23, 2001 restriction requirement. Therefore, 35 U.S.C 121, third sentence prohibits the Examiner from using application 09/855,817 as a reference for a double patenting rejection.

The 35 U.S.C. 121, third sentence, bar to double patenting rejections is also found in Section 804.01 of the M.P.E.P. (Original Eight Edition, August, 2001) which states in relevant part:

> The third sentence of 35 U.S.C. 121 prohibits the use of a patent issuing on an application with respect to which a requirement for restriction has been made, or on an application filed as a result of such a requirement, as a reference against any divisional application, if the divisional application is filed before the issuance of the patent.

Because the Examiner's double patenting rejection is erroneous both as a matter of a law and as a matter of patent examining procedure, Applicant respectfully requests that the rejection be withdrawn.

Rejection of Claims Under 35 U.S.C. 103(a)

The Examiner has rejected claims 1, 3-5, 28, 29, 33, 34, 54, 56, 68 and 60-65 under 35 U.S.C. 103(a) as being unpatentable over Char *et al.* (USP 5,157,466) in view of Ishimaru *et al.* (USP 5,883,051).

The Examiner bases the rejection on the contention that it would have been obvious to make part of the structure taught by Char *et al.* mesoscopic (*e.g.*, 310 of Char *et al.* Fig. 14) as a design alternative in view of the five micron neck disclosed in Ishimaru *et al.* The rejection is respectfully traversed. First, Char *et al.* does not teach or suggest an island. Second, there is no suggestion or motivation to modify or combine the teachings of Char *et al.* and Ishimaru *et al.* in order to achieve the claimed invention. Third, even if the failure to identify a suggestion or motivation to combine such references were overlooked, the combined structure would still not have a mesoscopic island as recited in independent claims 1, 28, 60 and 64. It is simply not possible for a five-micron wide bank to support discrete quantum states (*i.e.*, to be mesoscopic). Thus, contrary to the Examiner's contention, the devices in Char *et al.* cannot be made mesoscopic as a design alternative. These grounds for traversal will now be addressed in turn.

With respect to the first ground for traversal, the Examiner contends that Char *et al.* teaches the formation of a grain boundary JJ of high temperature superconductor material where a region 310 is connected to a body 312. Applicant respectfully submits that region 310 is not an island, much less a mesoscopic island. Rather, region 310 is a lead of a dc Superconducting Quantum Interference Device (SQUID). A dc SQUID can be made by patterning a superconducting thin film using photolithography to create parallel Josephson junctions as shown in Figure 2 below. In Char, current flows in one end of the dc SQUID and out the other end of region 310.

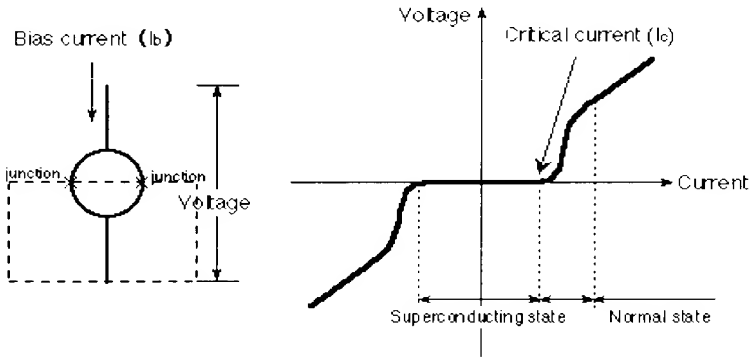

FIGURE 2

When bias current (Ib) is applied to the SQUID, voltage through the SQUID is zero when the current is less than the critical current of the Josephson junctions. When bias current exceeds critical current (Ic), the SQUID turns to the normal state and voltage is produced. Element 310 (Fig. 14 of Char *et al.*) refers to the entire portion of the circuit enclosed in the dashed box in Figure 2 above. This can be seen by inspection of Figure 14. In Figure 14, line 314 defines the grain boundary between regions 310 and 312. The two Josephson junctions found in a dc SQUID form an interface 314 between sections 312 and 310 at points 1000-1 and 1000-2 in the reproduction of Char *et al.*, Figure 14 below:

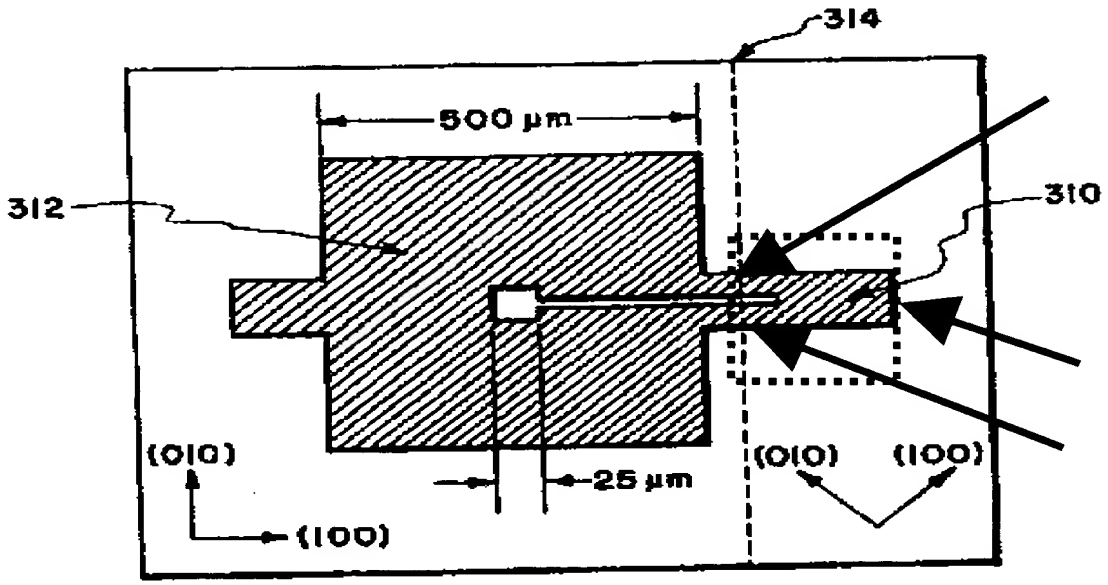

FIG. 14

Thus, the boxed region 1002 in the reproduction of Char *et al.* Fig. 14 is the same as the boxed region in Figure 2 above. As such, region 310 is not an island, but rather an electronic lead as well as an interface with two Josephson junctions (1000-1 and 1000-2).

With respect to the second ground for traversal, no motivation to combine references, the Examiner admits that Char *et al.* does not teach or suggest making part of the devices disclosed in Char *et al.* mesoscopic. To remedy this deficiency in Char *et al.*, the Examiner identifies a neck in Ishimaru *et al.* that is five microns wide. The Examiner states that, in view of the five-micron neck in Ishimaru *et al.*, it would have been obvious to make part of the Char *et al.* structure mesoscopic as a design alternative. However, there is absolutely no motivation to incorporate the five-micron dimension into the Char *et al.* device. If region 310 of the dc SQUID illustrated in Figure 14 of Char *et al.* were reduced to the dimensions taught by Ishimaru *et al.*, it would not improve the function of the dc SQUID. The mere fact that references can be modified or combined does not render the resultant modification or combination obvious unless the prior art also suggests the desirability of the modification or combination. MPEP § 2143.01. Here, there is no suggestion in Ishimaru *et al.* or Char *et al.* that such a modification would be desirable.

Furthermore, one of skill in the art would not be motivated to combine Ishimaru *et al.* and Char *et al.* because the current densities of the Ishimaru *et al.*

junctions are two orders of magnitude less than the current densities of the Char *et al.* devices. Thus, any combination of Char *et al.* and Ishamaru *et al.* would be impractical for the purposes set forth in Char *et al.* Specifically, Char *et al.*, column 3, lines 12-19, indicates that the prior art has failed to achieve 1 x 10^6 amperes/cm^2 current densities. An academic paper, Ishimaru *et al.*, 1997, Physical Review B 55, 11851-11859, enclosed as Appendix F, describes more fully USP 5,883,051 to Ishimaru *et al.* On page 11855, column 1, the academic paper states that the current density of the Ishimaru *et al.* devices, J_c, is 4.4 x 10^4 Amp/cm^2.

Thirdly, even if lack of a suggestion or motivation to combine Char *et al.* and Ishimaru *et al.* and the failure of Char *et al.* to teach an island were overlooked, the combination of Char *et al.* and Ishimaru *et al.* would still not include a mesoscopic island. Yet, a mesoscopic island is recited in claims 1, 28, 60 and 64. Ishimaru *et al.* merely teaches patterning at the five-micron level. But it is simply not possible for a five-micron wide bank to support discrete quantum states (*i.e.*, to be mesoscopic). In describing an exemplary embodiment, page 7, line 29, through page 8, line 2, of the specification details a mesoscopic island (Fig. 1A, element 120) having a width W (specification, Fig. 1A) of about 0.2 microns or less, a length L (specification, Fig. 1A) of about 0.5 microns or less, and a thickness of about 0.2 microns or less. The amount of capacitance stored by an island is a function of the width W (as shown in Fig. 1A of the instant application) of the island. A material having a width W on the order of five microns would have too much capacitance to be mesoscopic. No materials have been discovered to date that can support a mesoscopic system having a width W of five microns. Therefore, the combination of Char *et al.* and Ishimaru *et al.* does not teach or suggest a mesoscopic island as recited in claims 1, 28, 60 and 64.

For the three reasons identified above, Char *et al.*, either alone or in combination with Ishimaru *et al.*, does not anticipate claims 1, 28, 60 or 64. Because claims 3-5, 29, 33, 34, 54, 56, 58, 61-63, and 65 ultimately depend from claims 1, 28, 60 and 64, Char *et al.* in view of Ishimaru *et al.* does not anticipate these claims either.

Rejection of Claims Under 35 U.S.C. 103(a) Over Char et al. in View of Ishimaru et al. and further in view of Shnirman et al.

The Examiner has rejected claims 2, 30, 31, and 52 under 35 U.S.C. 103(a) as being unpatentable over Char *et al.* (USP 5,157,466) in view of Ishimaru *et al.* (USP

5,883,051) and further in view of Shnirman *et al.* (Physical Review B 57, 15400, 1998). Char *et al.*, either alone or in combination with Ishimaru *et al.*, does not anticipate claims 1, 28, 60 or 64 for the reasons discussed above. Shnirman merely teaches a SET coupled capacitively to a Josephson junction q-bit. As such, Shnirman *et al.* does not remedy the deficiencies identified in the combination of Char *et al.* and Ishimaru *et al.* For this reason, the combination of Char *et al.*, Ishimaru *et al.*, and Shnirman *et al.* does not render claims 1, 28, 60 or 64 obvious. Since claims 2, 30, 31, and 52 ultimately depend from 1, 28, 60 or 64, Char *et al.* in view of Ishimaru *et al.* and further in view of Shnirman *et al.* does not anticipate these claims either.

Rejection of Claims Under 35 U.S.C. 103(a) Over Char et al. in View of Ishimaru et al. and further in view of Baechtold et al.

The Examiner has rejected claims 6, 8-10, 35, 39, 40, 41, 53, 55, 57, and 59 under 35 U.S.C. 103(a) as being unpatentable over Char *et al.* (USP 5,157,466) in view of Ishimaru *et al.* (USP 5,883,051) and further in view of Baechtold *et al.* (USP 3,953,749). Char *et al.*, either alone or in combination with Ishimaru *et al.*, does not anticipate claims 1, 28, 60 or 64 for the reasons discussed above. Baechtold *et al.* merely teaches a binary circuit consisting of a series/parallel arrangement of Josephson junctions. As such, Baechtold *et al.* does not remedy the deficiencies identified in the combination of Char *et al.* and Ishimaru *et al.* For this reason, the combination of Char *et al.*, Ishimaru *et al.*, and Baechtold *et al.* does not render claims 1, 28, 60 or 64 obvious. Since claims 6, 8-10, 35, 39, 40, 41, 53, 55, 57, and 59 ultimately depend from 1, 28, 60 or 64, Char *et al.* in view of Ishimaru *et al.* and further in view of Baechtold *et al.* does not anticipate these claims either.

Rejection of Claims Under 35 U.S.C. 103(a) Over Char et al. in View of Ishimaru et al. and further in view of Baechtold et al. as well as Shnirman et al.

The Examiner has rejected claims 7, 11, 12-18, 36, 37, 42, 43, 45, 46, and 48-50 under 35 U.S.C. 103(a) as being unpatentable over Char *et al.* in view of Ishimaru *et al.* and further in view of Baechtold *et al.* as well as Shnirman *et al.* As previously discussed Char *et al.*, either alone or in combination with Ishimaru *et al.*, does not anticipate claims 1, 28, 60 or 64. Baechtold *et al.* and Shnirman *et al.* do not remedy the deficiencies identified in the combination of Char *et al.* and Ishimaru *et al.* For this reason, the combination of Char *et al.*, Ishimaru *et al.*, Baechtold *et al.*, and

Ishimaru *et al.* does not render claims 1, 28, 60 or 64 obvious. Since claims 7, 11, 12-18, 36, 37, 42, 43, 45, 46, and 48-50 ultimately depend from claims 1, 28, 60 or 64, the combination of all four references does not anticipate these claims either.

In light of the above remarks, the Applicant respectfully requests that the Examiner reconsider this application with a view towards allowance. The Examiner is invited to call the undersigned attorney if a telephone call could help resolve any remaining items.

Respectfully submitted,

PENNIE & EDMONDS LLP

By: 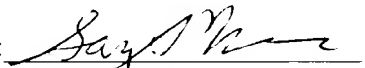

Gary S. Williams
Reg. No. 31,066

3300 Hillview Avenue
Palo Alto, CA 94304
Telephone: (650) 493-4935

APPENDIX A

CHANGES TO THE CLAIMS

The rewritten claims were revised as follows:

52. (Amended) The structure of claim 1, wherein a qubit is formed by the first bank, the mesoscopic island and the clean Josephson junction, and wherein each quantum state on the qubit is characterized by a clockwise or a counterclockwise [circulating] supercurrent that circulates in a plane in the vicinity of the clean Josephson junction.

53. (Amended) The quantum register of claim 8, wherein a plurality of qubits is formed by the plurality of mesoscopic islands, the bank, and the plurality of clean Josephson junctions, and wherein each quantum state on each respective qubit in said plurality of qubits is characterized by a clockwise or a counterclockwise [circulating] supercurrent that circulates in a plane in the vicinity of the Josephson junction in said respective qubit.

54. (Amended) The qubit of claim 28, wherein each quantum state on the qubit is characterized by a clockwise or a counterclockwise [circulating] supercurrent that circulates in a plane in the vicinity of the clean Josephson junction.

55. (Amended) The quantum register of claim 39, wherein a qubit is formed by each mesoscopic island in the at least one mesoscopic island together with the first bank and a Josephson junction in the at least one Josephson junction, and wherein each quantum state of each said qubit is characterized by a clockwise or a counterclockwise [circulating] supercurrent that circulates in a plane in the vicinity of the Josephson junction in said qubit.

Operation of universal gates in a solid state quantum computer based on clean Josephson junctions between d-wave superconductors

Alexandre Blais[a,*] and Alexandre M. Zagoskin[a,b,c,†]

[a] *Département de physique and Centre de Recherche en Physique du Solide, Université de Sherbrooke, Sherbrooke, Québec, J1K 2R1, Canada;*

[b] *DWS Inc., 119-1600 W. 6th Ave., Vancouver, B.C., Canada V6J 1R3;*

[c] *Physics and Astronomy Dept., U. of British Columbia, 6224 Agricultural Rd., Vancouver, B.C., V6T 1Z1, Canada*

The operation of solid state superconducting quantum computer based on clean Josephson junctions between two d-wave superconductors is considered. We show that freezing of passive qubits can be achieved using a dynamic global refocusing technique. Further, we demonstrate that a universal set of gates can be realized on this system, thereby proving its universality.

Quantum computation algorithms promise of enormous speed up in dealing with certain classes of problems [1,2] can only be realized if a quantum computing device is built on a scale of at least several thousand qubits. The inherent scalability of solid state devices and high level of expertise existing in industrial electronics and experimental mesoscopic physics make solid state-based quantum computers an attractive choice [3,4]. The problem of quantum coherence preservation in such devices, in the presence of macroscopic number of degrees of freedom, is difficult but at least theoretically solvable [3,4]. Moreover, in a recent experiment on a superconducting quantum dot (single electron transistor, SET) [5] coherent quantum beats were demonstrated in this mesoscopic system, which proves its suitability as a qubit prototype.

The coherent ground state and gapped excitation spectrum in superconductors make coherence preservation more achievable; there exist already several suggestions for quantum computers based on Josephson junctions and superconducting SETs [4,6,7].

In this paper we consider operation of quantum gates in a solid state quantum computer based on clean Josephson junctions between d-wave superconductors (i.e. ballistic DND or D-(grain boundary)-D junctions) [7]. Terminal B of the junction (Fig.1) is formed by a massive d-wave superconductor; in a multiple-qubit system, B would be a common "bus" bar. Terminal A is small enough to allow, when isolated, quantum phase fluctuations. It is essentially the sign of the superconducting phase difference φ between the terminals A and B that plays the role of "spin variable" of quantum computing. The collapse of the wave function is achieved by connecting terminal A to the equilibrium electron reservoir ("ground") through a parity key (superconducting SET), thus blocking phase fluctuations due to phase-number uncertainty relation [8]. Other parity keys, with different parameters, are used to link adjacent qubits, allowing for controllable entanglement. (A parity key only passes Cooper pairs, and only at a certain gate voltage V_g [9,10].)

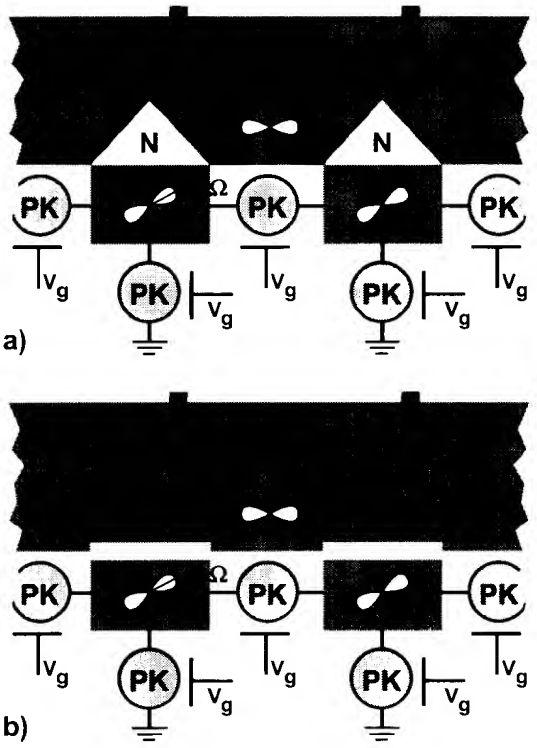

FIG. 1. a) Superconducting DND qubits: A,B are d-wave superconductors, N normal conductor, PK parity key, M scanning tip, Ω the mismatch angle between the lattices of A and B. The cut in B is here along (110) and (1$\bar{1}$0) directions. Positive lobes of d-wave order parameter are shaded. Two qubits are shown. b) Version of a) using grain boundary (G) junctions.

The dynamics of the device was considered in [7]. It is characterized by the phase difference φ between terminals A and B, which plays the role of the position of a quantum particle with mass $M \propto C$, C being the classical capacitance of the small terminal, in an effective two-well potential $U(\varphi)$ (Fig.2). It is the crucial advantage of clean DXD junctions, that the equilibrium phase $\pm\varphi_0$ continuously depends on the angle between crystal lattices of A and B (and therefore on the d-wave order pa-

rameters in these terminals) in the interval $[0, \pi[$ allowing for exponentially wide tuning of the tunneling rate [7,11]. Moreover,due to time-reversal symmetry breaking in the system, states with $\varphi = -\varphi_0$ and $\varphi = \varphi_0$ are always degenerate and can be used as basic $|0\rangle$ and $|1\rangle$ states of a qubit [6,7].

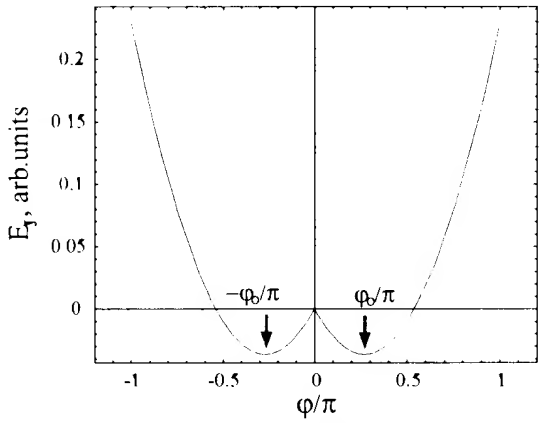

FIG. 2. Effective potential profile of the system. Minima at $\pm\varphi_0$ correspond to "up" and "down" pseudospin states of a qubit. The mismatch angle is $\Omega = \pi/8$.

The basic operations on a qubit are initialization, logical operations (quantum gates) and measurement. Measurement is a two-step procedure and can be performed simultaneously on all qubits or selectively on individual or groups of qubits. The first step, collapse of the wave function, is achieved by grounding terminal A. Readout is facilitated by the existence of small persistent currents and magnetic fluxes ($\lesssim \Phi_0$) which flow in opposite directions in the $|0\rangle$ and $|1\rangle$ states [7,11]. While too small to lead to unwanted inductive coupling between the qubits or decoherence, they can still be used to read out the state of the qubit once it was collapsed in one of the states with $\pm\varphi_0$, e.g. using a magnetic force microscope tip (which is removed during the computations). The estimated magnetic moment of order 10^5 to $10^6\mu_B$ is on the resolution limit of commercial magnetic force microscopes. The same property can be used to initialize individual qubits or whole registers, since this small coupling to an external field can put the qubit in a desired ($|0\rangle$ or $|1\rangle$) initial state.

Let us now describe how logical operations can be realized in this system. In order to maintain coherence, the qubit's electrodes A are isolated from ground while performing logical operations. The basic one-qubit logical operations are rotations around the x and z axes, $X(\theta)$ and $Z(\phi)$:

$$X(\theta) = e^{-i\sigma_x\theta/2}; \quad (1)$$

$$Z(\phi) = e^{-i\sigma_z\phi/2}. \quad (2)$$

Operation $X(\theta)$, where $\theta = 2t\Delta/\hbar$ and Δ are the tunneling matrix elements, is provided by natural quantum beats between the two basis states $|0\rangle$ and $|1\rangle$. On the other hand, an effective rotation around the z axis is realized by lifting the degeneracy of the basis states by an amount exceeding the tunneling width. Thereby tunneling between the basis states is suppressed and the natural oscillations between the basis states, $X(\theta)$, do not interfere with $Z(\phi)$ operations. The degeneracy between up/down states can be lifted in various ways. For example, it can be achieved by directly applying a localized magnetic field using a magnetic scanning tip. Other implementations will be discussed elsewhere.

As stated, the idle-state of this system corresponds to the logical operation $X(\theta)$. For a single qubit 'computer' this poses no problem as logical operations would be applied sequentially without waiting times ("do-nothing" periods). In the case that a "do-nothing" period is desired, one can choose this time to be a multiple of the oscillation period. Thus, using the above convention, this is equivalent to applying $X(2n\pi) = \mathbb{1}$, with n an integer and $\mathbb{1}$ the identity operator. The situation with more than one qubit is less straightforward. Here, we explicitly need passive qubits (qubits which undergo no logical operations) to be "frozen" during operation on the active qubits (qubits over which a logical operation is applied). For instance, if $Z(\phi)$ is applied on qubit one, the state of passive qubits must not change during this operation. Since the application time of logical gates will typically be incommensurate with the time required for $X(\theta)$ to be equal to $\mathbb{1}$, a scheme to freeze passive qubits is necessary. For this sake, it can be advantageous to have an idle-state where the energy of $|0\rangle$ and $|1\rangle$ are degenerate and tunneling is coherently blocked. One way to do this would be to temporarily enlarge the capacitance of electrode A by linking it with an external circuit as it was suggested by Ioffe *et. al.* in their "quiet-qubit" proposal [6]. However, such an approach brings the risk of losing coherence due to inelastic processes in the external normal circuits. On the other hand, making the external capacitor superconducting would bring uninvited evolution due to Josephson coupling between the external capacitor and electrode A.

Our suggestion is to employ instead a technique of dynamic global refocusing closely related to refocusing methods of NMR [12,13] and strong focusing of accelerators physics [14]. It relies on periodic perturbation of the two-well potential with amplitude δE slightly exceeding the tunneling width. In this scheme, the energy shift between the basis states is periodically varied from $-\delta E$ to δE. Explicitly, this corresponds to the pulse sequence

$$\cdots - Z(\delta E\tau/\hbar) - Z(-\delta E\tau/\hbar) - Z(\delta E\tau/\hbar) \quad \cdots \quad (3)$$

This results in a time dependent angle of rotation around the z axes which is given, in the ideal case, by a triangular function of period 2τ, the period of the refocusing sequence.

The evolution operator for a single qubit is then given, without approximation, by the Magnus expansion [13] : $U(t) = \exp[-i\sigma_z \int_0^t dt' \phi'(t')/2] = \exp[-i\sigma_z(\delta E\tau - \delta E\tau + \delta E\tau - \cdots)/2\hbar]$ so that, in the worst case, it is equal to $\exp[\pm i\sigma_z \delta E\tau/2\hbar]$. For τ sufficiently small this reduce to $U(t) \approx \mathbb{1}$. Hence, this yields a true idle-state as the information encoded by the qubits is not perturbed by tunneling nor by accumulation of relative phase between the basis states. The characteristic time scale of the refocusing pulse must be much less than the tunneling time (estimated in [7] as $\sim 10^{-8}$ s).

It was recently demonstrated (Viola and Lloyd [15] using the spin-boson model; Viola, Knill and Lloyd [16,17] under more general assumptions) that in the limit of *very* small τ, global refocusing leads to decoherence suppression in the σ_x and σ_y channels (phase decoherence) provided that $\phi = \pi$ and that delays between the refocusing pulses are smaller, or of the order of, the correlation time of the environment [18]. This correlation time is given by the inverse of a natural cutoff frequency $\tau_c \sim \omega_c^{-1}$ and determines the fastest time scale of the environment. In the case of semiconductor-based structures, where decoherence is due to phonons, τ_c is given by the inverse of the Debye frequency $\omega_c^{-1} \approx 10^{-13} s$ [16]. In the present situation, for τ to be very small requires $\tau \ll t_b$, where $t_b \sim l/v_f$ is the ballistic time (the time required for the formation of Andreev levels in the normal part of the system), l the size of the system and v_f the Fermi velocity. Taking $l \sim 10^3 \mathring{A}$ and $v_f \sim 10^7 cm/s$ [7], we arrive at $\tau \ll 10^{-12} s$, a similar estimate as in [16]. Another potentially dangerous source of decoherence comes from the localized degrees of freedom (nuclear spins and paramagnetic impurities) [19]. The estimates based on the central spin model [19] show that the relevant energies correspond to much longer times, in excess of 10^{-8} s. (The same estimate can be made for the decoherence time from these subsystems.) On the other hand, the dynamics of a spin bath is much more complicated than the one of oscillator bath or spin boson models, and its behavior under global refocusing should be a subject of special investigation.

Logical gates can be performed simultaneously with global refocusing pulses. Indeed, because the refocusing pulses obviously commute with $Z(\phi)$, refocusing can be applied to all qubits (actives and passives) while performing $Z(\phi)$ on a qubit or in parallel on a group of qubits. The evolution of the active qubits is then given by $\exp[-i\sigma_z(\int_0^t dt' \phi'(t') + \phi)/2] \approx Z(\phi)$. As a result, application of $Z(\phi)$ on, e.g. the first qubit, in combination with the refocusing sequence yields the desired overall action on all qubits : $Z(\phi) \otimes \mathbb{1} \otimes \cdots \otimes \mathbb{1}$. On the other hand, applying $X(\theta)$ reduces to stopping refocusing pulses on the active qubits for a determined period of time. This also yields the desired overall action [20].

In order to create entangled states, non-local gates are required. Such an entangling two-qubit operation is realized in this system by opening the parity key joining two adjacent qubits, Fig 1. With this parity key open, a Josephson current flows between states of opposite phases. Thus, the combination $|00\rangle$ and $|11\rangle$ carries no current while $|01\rangle$ and $|10\rangle$ does. As a result, states of opposite phase will differ from those of identical phase by a Josephson energy $E_J \sim 1 - \cos(2\varphi_0)$. The evolution of a pair of qubits in this situation then corresponds to a conditional phase shift (CP) and, to an irrelevant phase factor, can be represented in the computational basis $\{ |00\rangle, |01\rangle, |10\rangle, |11\rangle \}$ as

$$CP(\gamma) = \mathrm{Diag}(e^{i\gamma/2}, e^{-i\gamma/2}, e^{-i\gamma/2}, e^{i\gamma/2}), \qquad (4)$$

with $\gamma = E_J t/\hbar$. Because $CP(\gamma)$ is diagonal in the computational basis, it commutes with $Z(\phi)$. As a result, and under the assumption that the Josephson energy only weakly perturbs individual two-well potentials [21], the latter operation can be performed simultaneously with the global refocusing sequence. This condition can always be realized by tuning the gate voltage on the parity key, thus varying its transparency and Josephson energy.

Using the three basic operations defined above, it is possible to construct a Controlled-Not gate. This operation, denoted CN_{ij} where i and j are the control and target qubits respectively, acts as : $CN_{12}|i,j\rangle = |i, i \oplus j\rangle$, with $\oplus$ denoting addition modulo 2. Using the above expressions for one- and two-qubits gate, CN_{12} is realized in this system, up to an irrelevant global phase factor, by the following sequence

$$\begin{aligned} CN_{12} = e^{i5\pi/4} & X_2(\pi/2) Z_2(\pi/2) X_2(\pi/2) Z_2(\pi/2) \\ & Z_1(\pi/2) CP(\pi/2) X_2(\pi/2) Z_2(\pi/2) X_2(\pi/2). \end{aligned} \qquad (5)$$

In this expression, $X_i(\theta)$ ($Z_i(\phi)$) applies $X(\theta)$ ($Z(\phi)$) on the i^{th} qubit while leaving the others unchanged (e.g., $Z_1(\phi) = Z(\phi) \otimes \mathbb{1} \otimes \cdots \otimes \mathbb{1}$).

In the setup of figure 1, it is possible to apply two-qubit gates only to adjacent qubits. It is therefore necessary to introduce a swap operator, denoted SW_{ij}, which exchanges the states of qubits i and j. A swap on two adjacent qubits is realized by the following combination of Controlled-Not gates

$$SW_{12} = CN_{12} CN_{21} CN_{12}. \qquad (6)$$

Using this operator repeatedly, it is then possible to juxtapose any chosen pairs of qubits and, as a result, to apply Controlled-Not gates on any chosen pairs of qubits.

Because of the commutation relations between the Pauli operators, combinations of rotations around the x and z axes generate $SU(2)$, the group of 2 by 2 unitary matrices with determinant +1. Thus, it is possible to realize all one-qubit gates on this system. Furthermore, as been shown by Barenco *et. al*, the set of all single qubit gates and the Controlled-Not is complete for quantum computation [22]. It is therefore possible to generate

all of $SU(2^n)$ with proper sequences of gates in such a n-qubit DXD superconducting quantum computer.

In conclusion, we have shown that a solid state superconducting quantum computer suggested in [7] allows application of a complete set of quantum logical gates and is therefore a realization of a universal quantum computer.

Acknowledgements We are grateful to Martin Beaudry and Philip Stamp for helpful discussions and particularly to Serge Lacelle and André-Marie Tremblay for stimulating discussions and a critical reading of the manuscript. A.B. received support from FCAR. A.Z. was partially supported by FCAR and CIAR.

* Electronic address: ablais@physique.usherb.ca
† Electronic address: zagoskin@physics.ubc.ca

[1] P.W. Shor, Polynomial-time algorithms for prime factorization and discrete logarithms on a quantum computer, SIAM J. Comp. **26**, 1484 (1997).

[2] L.K. Grover, Quantum mechanics helps in searching for a needle in a haystack, Phys. Rev. Lett. **79**, 325 (1997).

[3] D.P. DiVincenzo, Quantum computing and single-qubit measurements using the spin filter effect, LANL e-print cond-mat/9810295 (1998); D.P. DiVincenzo and D. Loss, Quantum computers and quantum coherence, LANL e-print cond-mat/9901137 (1999).

[4] Y. Makhlin, G. Schön, and A. Shnirman, Josephson-junction qubits with controlled couplings, Nature (London) **398**, 305 (1999); G. Schön *et. al.*, Josephson-junction qubits and the readout process by single-electron transistors, LANL e-print cond-mat/9811029 (1998).

[5] Y. Nakamura, Y.A. Pashkin and J.S. Tsai, Coherent control of macroscopic quantum states in a single-Cooper-pair box, Nature (London) **398**, 786 (1999).

[6] L.B. Ioffe *et. al.*, Environmentally decoupled sds-wave Josephson junctions for quantum computing, Nature, **398**, 679 (1999).

[7] A.M. Zagoskin, A scalable, tunable qubit, based on a clean DND or grain boundary D-D junction, LANL e-print cond-mat/9903170 (1999).

[8] M. Tinkham, *Introduction to superconductivity*, 2nd ed., McGraw Hill, New York (1996)

[9] K. Matveev *et. al.*, Parity-induced suppression of the Coulomb blockade of Josephson tunneling, Phys. Rev. Lett. **70**, 2940 (1993).

[10] P. Joyez *et. al*, Observation of parity-induced suppression of Josephson tunneling in the superconducting single electron transistor, Phys. Rev. Lett **72**, 2548 (1994).

[11] A.M. Zagoskin and M. Oshikawa, Spontaneous magnetic flux and quantum noise in an annular mesoscopic SND junction, J.Phys.: Cond. Matter, **10**, L105 (1998).

[12] C.P. Slichter, *Principles of Magnetic Resonance*, 3rd ed., Springer-Verlag (1990).

[13] R.R. Ernst, G. Bodenhausen and A. Wokaun, *Principles of Nuclear Magnetic Resonance in One and Two Dimensions*, Clarendon Press, Oxford (1987).

[14] J.J. Livingood, *Principles of cyclic particle accelerators*, D. Van Nostrand, Princeton (1961), Ch.12.

[15] L. Viola and S. Lloyd, Dynamical suppression of decoherence in two-state quantum system, Phys. Rev. A **58**, 2733 (1998).

[16] L. Viola, E. Knill and S. Lloyd, Dynamical decoupling of open quantum systems, Phys. Rev. Lett. **82**, 2417 (1999).

[17] L. Viola, E. Knill and S. Lloyd, Universal control of decoupled quantum systems, LANL e-print quant-ph/9906094 (1999).

[18] Here $\sigma_{x,y}$-channels refer to the processes described by the corresponding Pauli matrices in the computational basis and involving coherent tunneling between its states (cf. Eq.(1)).

[19] N.V. Prokof'ev and P.C.E. Stamp, Theory of the spin bath, Rep. Prog. Phys. **63**, 669 (2000).

[20] Freezing of passive qubits during application of $Z(\phi)$ is unnecessary if the characteristic time of the z-rotation is much faster than the tunneling time. On the contrary, freezing cannot be avoided during $X(\theta)$ operations whatever its characteristic time compared to $Z(\phi)$.

[21] The critical Josephson current through the open parity key must be thus chosen to be much less than the one through the clean d-d boundary.

[22] A. Barenco, *et. al.*, Elementary gates for quantum computation, Phys. Rev. A **52**, 3457 (1995).

APPENDIX C

Courtesy copy of Blais and Zagoskin, arXiv:quant-ph/9905043 v.2 (April 7, 2000)

DICTIONARY OF

PHYSICS

EDITED BY

H. J. GRAY
C.M.G., M.Sc., LL.B., M.P.A(HARVARD),
M.INST.P., F.R.S.A.

ALAN ISAACS
PH.D., B.Sc., D.I.C., A.C.G.I.

LONGMAN

This new edition has been prepared and typeset by Market House Books Ltd

The work of revision and the preparation of new entries has been carried out by:

VALERIE ILLINGWORTH, M.PHIL., B.SC.
JOHN DAINTITH, PH.D., B.SC.
J W WARREN, PH.D.

Additional contributions have been made by:

RICHARD BATLEY, PH.D., M.INST.P.
COLIN BRETT, PH.D., B.A.
H M CLARKE, M.A., M.SC.
PROFESSOR A J H GODDARD, PH.D., M.I.MECH.E., F.INST. NUC.E., F.INST.P., M.S.R.P.
RICHARD RENNIE, PH.D., M.SC., B.SC.

NOTES

An asterisk indicates a cross reference.
An entry having an initial capital letter is either a proper name or a trade name.
Syn. is an abbreviation for "synonymous with".
All other abbreviations will be found in the Tables of SI Units (page 625) and the Table of Symbols for Physical Quantities (page 633).

ACKNOWLEDGEMENTS

The Table of Fundamental Constants has been selected from CODATA Bulletin No.63 (Nov. 1986)

Longman Group UK Limited,
Longman House, Burnt Mill, Harlow, Essex CM20 2JE, England
and Associated Companies throughout the world.

FIRST PUBLISHED 1958
SECOND EDITION 1975
THIRD EDITION 1991

BRITISH LIBRARY CATALOGUING IN PUBLICATION DATA
DICTONARY OF PHYSICS. — 3RD ED.
1. PHYSICS
I. ISAACS, ALAN II. GRAY, H.J.
530

ISBN 0–582–03797–2

Produced by Longman Singapore Publishers (Pte) Ltd.
Printed in Singapore

For electromagnetic deflection, the deflection sensitivity is expressed in metres per tesla of the deflecting magnetic field.

deflector coils Of a *cathode-ray tube employing electromagnetic deflection of the electron beam. The coils through which a current is passed to produce a magnetic field for the purpose of deflecting the beam of electrons. Two pairs of coils mounted close to the outside of the tube are usually employed and the pairs are described as *X* or *Y* according to whether they produce horizontal or vertical deflections of the beam respectively. The linear displacement of the luminous spot on the screen produced by one pair of coils is approximately proportional to the current in the coils. *Compare* deflector plates.

deflector plates Of a *cathode-ray tube employing electrostatic deflection of the electron beam. Electrodes to which a voltage is applied to produce an electrostatic field for the purpose of deflecting the beam of electrons. The electrodes are usually plates of metal and there are two pairs of them, the pairs being described as *X* or *Y* according to whether they produce horizontal or vertical deflections of the beam respectively. The deflector plates are mounted inside the tube. The linear displacement of the luminous spot on the screen produced by one pair of plates is approximately proportional to the voltage applied between the plates. *Compare* deflector coils.

de Forest, Lee (1873–1962) Amer. scientist who invented the three-electrode thermionic valve (triode) in 1907.

deformation potential The electric potential caused by mechanical deformation of the crystal lattice of *semiconductors and conductors. *See* piezoelectric effect.

degas *See* outgassing.

degaussing 1. Neutralization of the magnetization of a ship by surrounding it with a system of current-carrying cables that set up an exactly equal and opposite field.

2. In colour television, the use of a system of coils to neutralize the earth's magnetic field thus preventing the formation of colour fringes on the image.

degeneracy 1. A condition that arises when an atom or molecule has two or more quantum states with the same energy. The states are said to be *degenerate*. *See* statistical weight.

2. The condition of matter at high density, particularly at low temperatures, when the energy distribution of one or more types of particle departs greatly from the classical form, so that the exact equations of *quantum statistics must be used. This applies to the valence electrons in solids, to the electrons (and sometimes other particles) in highly condensed stellar interiors, and to superfluid liquid helium. *See* degenerate gas.

degenerate *See* characteristic function; statistical weight.

degenerate gas A gas in which the concentration of particles is sufficiently high for the Maxwell–Boltzman distribution (*see* distribution of velocities) not to hold; the behaviour of the gas is then controlled by *quantum statistics.

The pressure in a degenerate gas consisting of *fermions is called the *degeneracy pressure*; this exceeds the thermal pressure because according to the *Pauli exclusion principle particles very close together must possess different momenta and according to the *uncertainty principle the difference in momentum is inversely proportional to the distance between them. Thus, in a high-density gas the relative momentum of the particles is high and unlike thermal pressure does not tend to zero as the temperature tends to absolute zero. *White dwarfs and *neutron stars are thought to be supported against collapsing gravitationally by the degeneracy pressure of their electrons and neutrons, respectively.

degenerate level An *energy level of a quantum mechanical system that corresponds to more than one quantum state.

degenerate semiconductor A *semiconductor with the *Fermi level located inside either the *valence band or conduction band (*see* energy bands). The material is essentially metallic in behaviour over a wide temperature range.

degradation 1. The decrease in the availability of energy for doing work, as a result of the increase of *entropy within a closed system. (*See* thermodynamics.)

2. The loss of energy of a beam of particles or an isolated particle passing through matter as a result of the interaction of the particles with the matter.

degree 1. A unit of temperature difference. The Celsius and Fahrenheit degrees were formerly defined as 1/100th and 1/180th respectively of the temperature difference between the ice and steam points, so that 1 °C = $\frac{5}{9}$ °F. The unit of *thermodynamic temperature, no longer called a degree, is the *kelvin.

2. (math.) The rank of an equation or expression as determined by the highest power of the unknown or variable quantity. The degree of a curve or surface is that of the equation expressing it.

3. *See* electrical degrees.

degree Celsius Symbol: °C. A unit used in expressing temperatures on the *Celsius scale. It is now an *SI unit, defined in terms of thermodynamic temperature, one degree Celsius being equal to one *kelvin. (*See also* degree.) It was formerly called the *degree centigrade*.

degrees of freedom 1. The number of degrees of freedom of a mechanical system is equal to the number of independent variables needed to describe its configuration; e.g. a system consisting of two particles connected by a rigid bar has 5 degrees of freedom since 5 coordinates (3 of the mass centre or

tinctive features are very similar to those observed in the ~2500-Ma Mt. McRae Shale, and their age is supported by more thorough analytical protocols (*24*). The discovery and careful analysis of biomarkers in rocks of still greater age and of different Archean environments will potentially offer new insights into early microbial life and its evolution.

References and Notes

1. J. W. Schopf, *Science* **260**, 640 (1993).
2. M. R. Walter, in *Earth's Earliest Biosphere*, J. W. Schopf, Ed. (Princeton Univ. Press, Princeton, NJ, 1983), pp. 187–213.
3. S. J. Mojzsis *et al.*, *Nature* **384**, 55 (1996)
4. J. M. Hayes, I. R. Kaplan, K. W. Wedeking, in (*2*), pp. 93–134.
5. F. D. Mango, *Nature* **352**, 146 (1991).
6. A. Dutkiewicz, B. Rasmussen, R. Buick, *ibid.* **395**, 885 (1998).
7. K. E. Peters and J. M. Moldowan, *The Biomarker Guide* (Prentice-Hall, Englewood Cliffs, NJ, 1993).
8. R. C. Morris, *Precambrian Res.* **60**, 243 (1993).
9. A. F. Trendall, D. R. Nelson, J. R. de Laeter, S. W. Hassler, *Aust. J. Earth Sci.* **45**, 137 (1998)
10. N. T. Arndt, D. R. Nelson, W. Compston, A. F. Trendall, A. M. Thorne, *ibid.* **38**, 261 (1991).
11. R. E. Smith, J. L. Perdrix, T. C. Parks, *J. Petrol.* **23**, 75 (1982).
12. J. M. Gressier, thesis, University of Sydney, Sydney, Australia (1996).
13. T. C. Hoering and V. Navale, *Precambrian Res.* **34**, 247 (1987).
14. D. R. Nelson, A. F. Trendall, J. R. de Laeter, N. J. Grobler, I. R. Fletcher, *ibid.* **54**, 231 (1992).
15. R. E. Summons, T. G. Powell, C. J. Boreham, *Geochim. Cosmochim. Acta* **52**, 1747 (1988).
16. R. E. Summons and M. R. Walter, *Am. J. Sci.* **290A**, 212 (1990).
17. T. C. Hoering, *Carnegie Inst. Wash. Yearb.* **64**, 215 (1965); *ibid.* **65**, 365, (1966).
18. G. A. Logan, J. M. Hayes, G. B. Heishima, R. E. Summons, *Nature* **376**, 53 (1995); G. A. Logan, R. E. Summons, J. M. Hayes, *Geochim. Cosmochim. Acta* **61**, 5391 (1997).
19. G. A. Logan *et al.*, *Geochim. Cosmochim. Acta*, **63**, 1345 (1999).
20. S. J. Rowland, *Org. Geochem.* **15**, 9 (1990).
21. J. M. Hayes, in *Early Life on Earth*, Nobel Symposium No. 84, S. Bengtson, Ed. (Columbia Univ. Press, New York, 1994), pp. 220–236.
22. J. W. Schopf and B. M. Packer, *Science* **237**, 70 (1987).
23. R. Buick, *ibid.* **255**, 74 (1992).
24. R. E. Summons, L. L. Jahnke, J. M. Hope, G. A. Logan, *Nature*, in press.
25. H. D. Holland and N. J. Beukes, *Am. J. Sci.* **290A**, 1 (1990); A. H. Knoll and H. D. Holland, in *Effects of Past Global Change on Life*, S. M. Stanley, Ed. (National Academy Press, Washington, DC, 1995), pp. 21–33.
26. P. S. Braterman, A. G. Cairns-Smith, R. W. Sloper, *Nature* **303**, 163 (1983).
27. F. Widdel *et al.*, *ibid.* **362**, 834 (1993).
28. P. Cloud, *Science* **160**, 729 (1968); *Econ. Geol.* **68**, 1135 (1973).
29. G. Ourisson, M. Rohmer, K. Poralla, *Annu. Rev. Microbiol.* **41**, 301 (1987).
30. W. Kohl, A. Gloe, H. Reichenbach, *J. Gen. Microbiol.* **129**, 1629 (1983).
31. T.-M. Han and B. Runnegar, *Science* **257**, 232 (1992); A. H. Knoll, *ibid.* **256**, 622 (1992).

32. Supported by the Studienstiftung des Deutschen Volkes (J.J.B.) and American Chemical Society Petroleum Research Fund (R.B.). We thank J. Gressier and RioTinto Exploration for samples, the AGSO Isotope & Organic Geochemistry staff for technical assistance, J. Kamprad for x-ray diffraction analyses, T. Blake, D. Des Marais, L. L. Jahnke, C. J. Boreham, D. S. Edwards, T. G. Powell, D. E. Canfield, and M. R. Walter for advice, and J. M. Hayes, A. Knoll, and an anonymous reviewer for their thoughtful comments. G.A.L. and R.E.S. publish with the permission of the Executive Director of AGSO.

19 May 1999; accepted 13 July 1999

REPORTS

Josephson Persistent-Current Qubit

J. E. Mooij,[1,2]* T. P. Orlando,[2] L. Levitov,[3] Lin Tian,[3] Caspar H. van der Wal,[1] Seth Lloyd[4]

A qubit was designed that can be fabricated with conventional electron beam lithography and is suited for integration into a large quantum computer. The qubit consists of a micrometer-sized loop with three or four Josephson junctions; the two qubit states have persistent currents of opposite direction. Quantum superpositions of these states are obtained by pulsed microwave modulation of the enclosed magnetic flux by currents in control lines. A superconducting flux transporter allows for controlled transfer between qubits of the flux that is generated by the persistent currents, leading to entanglement of qubit information.

In a quantum computer, information is stored on quantum variables such as spins, photons, or atoms (*1*–*3*). The elementary unit is a two-state quantum system called a qubit. Computations are performed by the creation of quantum superposition states of the qubits and by controlled entanglement of the information on the qubits. Quantum coherence must be conserved to a high degree during these operations. For a quantum computer to be of practical value, the number of qubits must be at least 10^4. Qubits have been implemented in cavity quantum electrodynamics systems (*4*), ion traps (*5*), and nuclear spins of large numbers of identical molecules (*6*). Quantum coherence is high in these systems, but it seems difficult or impossible to realize the desired high number of interacting qubits. Solid state circuits lend themselves to large-scale integration, but the multitude of quantum degrees of freedom leads in general to short decoherence times. Proposals have been put forward for future implementation of qubits with spins of individual donor atoms in silicon (*7*), with spin states in quantum dots (*8*), and with d-wave superconductors (*9*); the technology for practical realization still needs to be developed.

In superconductors, all electrons are condensed in the same macrosopic quantum state, separated by a gap from the many quasi-particle states. This gap is a measure for the strength of the superconducting effects. Superconductors can be weakly coupled with Josephson tunnel junctions (regions where only a thin oxide separates them). The coupling energy is given by $E_J(1 - \cos \gamma)$, where the Josephson energy E_J is proportional to the gap of the superconductors divided by the normal-state tunnel resistance of the junction and γ is the gauge-invariant phase difference of the order parameters. The current through a Josephson junction is equal to $I_c \sin \gamma$, with $I_c = (2e/\hbar)\, E_J$, where e is the electron charge and $\hbar$ is Planck's constant divided by 2π. In a Josephson junction circuit with small electrical capacitance, the numbers of excess Cooper pairs on islands n_i, n_j and the phase differences γ_i, γ_j are related as noncommuting conjugate quantum variables (*10*). The Heisenberg uncertainty between phase and charge and the occurrence of quantum superpositions of charges as well as phase excitations (vortexlike fluxoids) have been demonstrated in experiments (*11*). Coherent charge oscillations in a superconducting quantum box have recently been observed (*12*). Qubits for quantum computing based on charge states have been suggested (*13*, *14*). However, in actual practice, fabricated Josephson circuits exhibit a high level of static and dynamic charge noise due to charged impurities. In contrast, the magnetic background is clean and stable. Here, we present the design of a qubit with persistent currents of opposite sign as its basic states. The qubits

[1]Department of Applied Physics and Delft Institute for Microelectronics and Submicron Technologies, Delft University of Technology, Post Office Box 5046, 2600 GA Delft, Netherlands. [2]Department of Electrical Engineering and Computer Science, [3]Department of Physics and Center for Materials Science and Engineering, [4]Department of Mechanical Engineering, Massachusetts Institute of Technology, Cambridge, MA 02139, USA.

*To whom correspondence should be addressed. E-mail: mooij@qt.tn.tudelft.nl

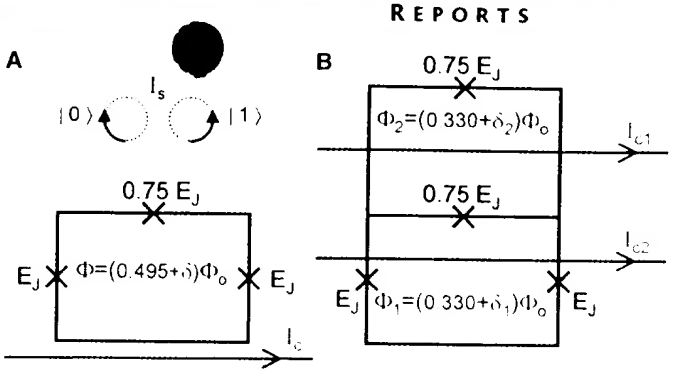

Fig. 1. Persistent current qubit. **(A)** Three-junction qubit. A superconducting loop with three Josephson junctions (indicated with crosses) encloses a flux that is supplied by an external magnet. The flux is $f\Phi_o$, where Φ_o is the superconducting flux quantum and f is 0.495. Two junctions have a Josephson coupling energy E_J, and the third junction has αE_J, where $\alpha = 0.75$. This system has two (meta)stable states |0> and |1> with opposite circulating persistent current. The level splitting is determined by the offset from $\Phi_o/2$ of the flux. The barrier between the states depends on the value of α. The qubit is operated by resonant microwave modulation of the enclosed magnetic flux by a superconducting control line (indicated in red). **(B)** Four-junction qubit. The top junction of (A) is replaced by a parallel junction (SQUID) circuit. There are two loops with equal areas; a magnet supplies a static flux $0.330\Phi_o$ to both. Qubit operations are performed with currents in superconducting control lines (indicated in red) on top of the qubit, separated by a thin insulator. The microwave current I_{c1} couples only to the bottom loop and performs qubit operations as in (A). I_{c2} couples to both loops; it is used for qubit operations with suppressed σ_z action and for an adiabatic increase of the tunnel barrier between qubit states to facilitate the measurement.

can be driven individually by magnetic microwave pulses; measurements can be made with superconducting magnetometers [superconducting quantum interference devices (SQUIDs)]. They are decoupled from charges and electrical signals, and the known sources of decoherence allow for a decoherence time of more than 1 ms. Switching is possible at a rate of 100 MHz. Entanglement is achieved by coupling the flux, which is generated by the persistent current, to a second qubit. The qubits are small (of order 1 μm), can be individually addressed, and can be integrated into large circuits.

Our qubit in principle consists of a loop with three small-capacitance Josephson junctions in series (Fig. 1A) that encloses an applied magnetic flux $f\Phi_o$ (Φ_o is the superconducting flux quantum $h/2e$, where h is Planck's constant); f is slightly smaller than 0.5. Two of the junctions have equal Josephson coupling energy E_J; the coupling in the third junction is αE_J, with $0.5 < \alpha < 1$. Useful values are $f = 0.495$ and $\alpha = 0.75$ (as chosen in Fig. 1A). This system has two stable classical states with persistent circulating currents of opposite sign. For $f = 0.5$, the energies of the two states are the same; the offset from 0.5 determines the level splitting. The barrier for quantum tunneling between the states depends strongly on the value of α. The four-junction version (Fig. 1B) allows modulation of this barrier in situ. Here, the third junction has been converted into a parallel circuit of two junctions, each with a coupling energy αE_J. The four-junction qubit behaves as the three-junction circuit of Fig. 1A, with an enclosed flux $(f_1 + f_2/2)\Phi_o$ and a third-junction (SQUID) strength $2\alpha E_J \cos(f_2\pi)$. The constant fluxes $f\Phi_o$, $f_1\Phi_o$, and $f_2\Phi_o$ are supplied by an external, static, homogeneous magnetic field. Control lines on a separate fabrication level couple inductively to individual qubit loops. All operations on qubits are performed with currents in the control lines.

When γ_1 and γ_2 are the gauge-invariant phase differences across the left and right junctions, the Josephson energy of the four-junction qubit U_J is

$$U_J/E_J = 2 + 2\alpha - \cos\gamma_1 - \cos\gamma_2 - 2\alpha\cos(f_2\pi)\cos(2f_1\pi + f_2\pi + \gamma_1 - \gamma_2) \quad (1)$$

In this expression, the self-generated flux has been neglected. Although this flux will be used for coupling of qubits, it is much smaller than the flux quantum and only slightly changes the picture here. U_J is 2π periodic in γ_1 and γ_2 (Fig. 2A) for the parameter values $\alpha = 0.75$ and $f_1 = f_2 = 0.330$. Each unit cell has two minima L_{ij} and R_{ij} with left- and right-handed circulating currents of about $0.75I_o$ at approximate γ_1,γ_2 values of $\pm 0.27\pi$. The minima would have been symmetric for $2f_1 + f_2 = 1$, which corresponds to a three-junction loop enclosing half a flux quantum. The set of all L minima yields one qubit state and the set of R minima the other. In γ_1,γ_2 space, there are saddle-point connections between L and R minima as indicated with red (intracell, in) and blue lines (intercell, out). Along such trajectories, the system can tunnel between its macroscopic quantum states. The Josephson energy along the trajectories is plotted in Fig. 2B. The saddle-point energies U_{in} and U_{out} depend on α and f_2; lower SQUID coupling gives lower U_{in} but higher U_{out}. For $2\alpha\cos(f_2\pi) < 0.5$, the barrier for intracell tunneling has disappeared, and there is only one minimum with zero circulating current.

Motion of the system in γ_1,γ_2 space can be discussed in analogy with motion of a mass-carrying particle in a landscape with periodic potential energy. Motion in phase space leads to voltages across junctions. The kinetic energy is the associated Coulomb charg-

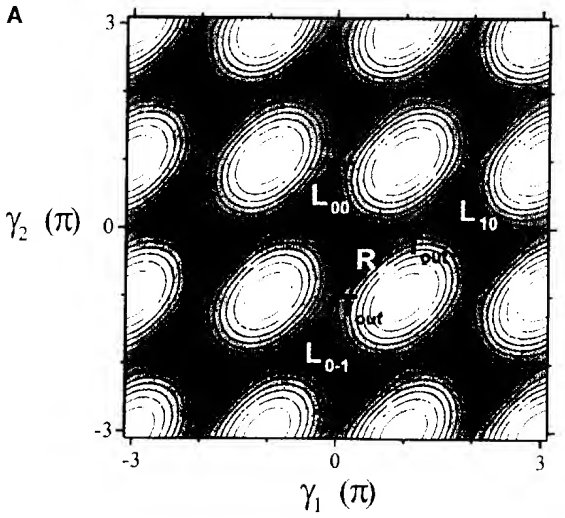

Fig. 2. Josephson energy of qubit in phase space. **(A)** Energy plotted as a function of the gauge-invariant phase differences γ_1 and γ_2 across the left and right junctions of Fig. 1A. The energy is periodic with period 2π. There are two minima in each unit cell, for the center cell indicated with L_{00} and R_{00}. The trajectory between L_{00} and R_{00} is indicated in red; the trajectories between R_{00} and minima in next-neighbor cells L_{10} and L_{0-1} are indicated in blue. **(B)** Energy along the red and a blue trajectory of (A). For the parameters chosen, the blue saddle point is substantially higher than the red saddle point. As a result, tunneling from cell to cell is suppressed and the qubit is decoupled from electrical potentials. (solid lines) $I_{c1} = I_{c2} = 0$ (see Fig. 1B). (dashed lines) Control current I_{c2} reduces the flux in the SQUID loop by $\delta_2 = -0.02$ times the flux quantum. Similarly, when α is increased (decreased) from 0.75, the red saddle point goes up (down), whereas the blue saddle point goes down (up).

ing energy of the junction capacitances. The mass is proportional to the junction capacitance C because other capacitance elements are small. The effective mass tensor has principal values M_a and M_b in the $\gamma_1 - \gamma_2 = 0$ and $\gamma_1 + \gamma_2 = 0$ directions. For the chosen values of the circuit parameters, these principal values are $M_a = \hbar^2/(4E_C)$ and $M_b = \hbar^2/(E_C)$, where the charging energy is defined as $E_C = e^2/2C$. The system will perform plasma oscillations in the potential well with frequencies $\hbar\omega_b \approx 1.3(E_C E_J)^{1/2}$ and $\hbar\omega_a \approx 2.3(E_C E_J)^{1/2}$. The tunneling matrix elements can be estimated by calculation of the action in the Wentzel-Kramers-Brillouin approximation. For tunneling within the unit cell between the minima L and R, the matrix element is $T_{in} \approx \hbar\omega_b \exp[-0.64(E_J/E_C)^{1/2}]$; for tunneling from cell to cell, the matrix element is $T_{out} \approx 1.6\hbar\omega_b \exp[-1.5(E_J/E_C)^{1/2}]$. For the qubit, a subtle balance has to be struck: The plasma frequency must be small enough relative to the barrier height to have well-defined states with a measurable circulating current but large enough (small enough mass) to have substantial tunneling. The preceding qualitative discussion has been confirmed by detailed quantitative calculations in phase space and in charge space (*15*). From these calculations, the best parameters for qubits can be determined. In practice, it is possible to controllably fabricate aluminum tunnel junctions with chosen E_J and E_C values in a useful range.

It is strongly desirable to suppress the intercell tunneling T_{out}. This suppression leads to independence from electrical potentials, even if the charges on the islands are conjugate quantum variables to the phases. The qubit system in phase space is then comparable to a crystal in real space with nonoverlapping atomic wave functions. In such a crystal, the electronic wave functions are independent of momentum; similarly, charge has no influence in our qubit.

Mesoscopic aluminum junctions can be reliably fabricated by shadow evaporation with critical current densities up to 500 A/cm^2. In practice, a junction of 100 nm^2 by 100 nm^2 has E_J around 25 GHz and E_C around 20 GHz. A higher E_J/E_C ratio can be obtained by increasing the area to which E_J is proportional and E_C is inversely proportional. A practical qubit would, for example, have junctions with an area of 200 nm^2 by 400 nm^2, $E_J \sim 200$ GHz, $E_J/E_C \sim 80$, level splitting $\Delta E \sim 10$ GHz, barrier height around 35 GHz, plasma frequency around 25 GHz, and tunneling matrix element $T_{in} \sim 1$ GHz. The matrix element for undesired tunneling T_{out} is smaller than 1 MHz. The qubit size would be of order 1 μm; with an estimated inductance of 5 pH, the flux generated by the persistent currents is about $10^{-3}\Phi_o$.

To calculate the dependence of the level splitting on f_1 and f_2, we apply a linearized approximation in the vicinity of $f_1 = f_2 = 1/3$, defining F as the change of U_J away from the minimum of $U_J(\gamma_1,\gamma_2)$. This yields $F/E_J = 1.2[2(f_1 - 1/3) + (f_2 - 1/3)]$. The level splitting without tunneling would be $2F$. With tunneling, symmetric and antisymmetric combinations are created; the level splitting is now $\Delta E = 2(F^2 + T_{in}^2)^{1/2}$. As long as $F \gg T_{in}$, the newly formed eigenstates are localized in the minima of $U_J(\gamma_1,\gamma_2)$.

We discuss qubit operations for the four-junction qubit. They are driven by the currents I_{ca} and I_{cb} in the two control lines (Fig. 1B). The fluxes induced in the two loops, normalized to the flux quantum, are $\delta_1 = (L_{a1}I_{ca} + L_{b1}I_{cb})/\Phi_o$ and $\delta_2 = (L_{a2}I_{ca} + L_{b2}I_{cb})/\Phi_o$. The control line positions are chosen such that $L_{a2} = 0$ and $L_{b2} = -2L_{b1}$. When the two loops have equal areas, $f_1 = f_2$ for zero control current. We assume that the qubit states are defined with zero control current and that δ_1 and δ_2 act as perturbations to this system. The effective Hamiltonian operator (H_{op}) in terms of Pauli spin matrices σ_x and σ_z for the chosen parameters is about

$$H_{op}/\Delta E \approx (80\delta_1 + 42\delta_2)\sigma_z - (9.2\delta_1 + 8.3\delta_2)\sigma_x \quad (2)$$

The numerical prefactors follow from the variational analysis of the influence of δ_1 and δ_2 on the tunnel barrier and the level splitting. The terms that contain σ_x can be used to induce Rabi oscillations between the two states, applying microwave pulses of frequency $\Delta E/h$. There are two main options, connected to one of the two control lines. Control current I_{ca} changes δ_1, which leads to a Rabi oscillation (σ_x term) as well as a strong modulation of the Larmor precession (σ_z term). As long as the Rabi frequency is far enough below the Larmor frequency, this is no problem. For $\delta_1 = 0.001$, the Rabi frequency is 100 MHz. This mode is the only one available for the three-junction qubit and is most effective near the symmetry point $f = 0.5$ or $f_1 = f_2 = 1/3$. Control current I_{cb} is used to modulate the tunnel barrier. Here, the σ_z action is suppressed by means of the choice $L_{b2}/L_{b1} = \delta_2/\delta_1 = -2$. However, a detailed analysis shows that with δ_2 modulation, it is easy to excite the plasma oscillation with frequency ω_b. One has to restrict δ_2 to remain within the two-level system. Values of 0.001 for δ_1 or δ_2 correspond to about 50-pW microwave power at 10 GHz in the control line. These numbers are well within practical range.

Two or more qubits can be coupled by means of the flux that the circulating persistent current generates. The current is about 0.3 μA, the self-inductance of the loop is about 5 pH, and the generated flux is about $10^{-3}\Phi_o$. When a superconducting closed loop (a flux transporter) with high critical current is placed on top of both qubits, the total enclosed flux is constant. A flux change $\Delta\Phi$ that is induced by a reversal of the current in one qubit leads to a change of about $\Delta\Phi/2$ in the flux that is enclosed by the other qubit. One can choose to couple the flux, generated in the main loop of qubit 1, to the main loop of qubit 2 ($\sigma_z \otimes \sigma_z$ coupling) or to the SQUID loop of qubit 2 ($\sigma_z \otimes \sigma_x$ coupling). A two-qubit gate operation is about as efficient as a single qubit operation driven with $\delta_1 = 0.001$. An example of a possible controlled-NOT operation with fixed coupling runs as follows: The level splitting of qubit 2 depends on the state of qubit 1, the values are ΔE_{20} and ΔE_{21}. When Rabi microwave pulses, resonant with ΔE_{21}, are applied to qubit 2, it will only react if qubit 1 is in its $|1\rangle$ state. In principle, qubits can be coupled at larger distances. An array scheme as proposed by Lloyd (*1*, *3*), where only nearest neighbor qubits are coupled, is also very feasible. It is possible to create a flux transporter that has to be switched on by a control current (Fig. 3)

The typical switching times for our qubit are 10 to 100 ns. To yield a practical quantum computer, the decoherence time should be at least 100 μs. We can estimate the influence of known sources of decoherence for our system, but it is impossible to determine the real decoherence time with certainty, except by measurement. We discuss

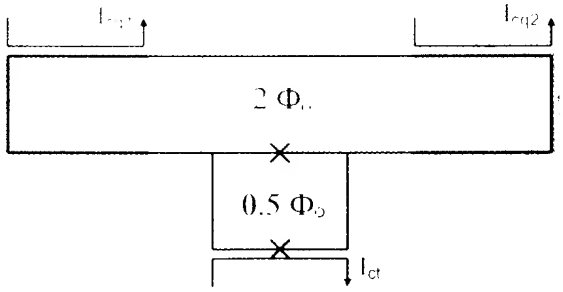

Fig. 3. Switchable qubit coupler. A superconducting flux transporter (blue) is placed on top of two qubits, separated by a thin insulator. The transporter is a closed loop that contains two Josephson junctions in parallel (SQUID) with high critical current. In the off state, the two loops of the transporter contain an integer number of flux quanta (main loop) and half a flux quantum (SQUID loop), supplied by a permanent magnet. The current response to a flux change is very small. In the on state, the flux in the SQUID loop is made integer by means of a control current I_{ct} (red). As the transporter attempts to keep the flux in its loop constant, a flux change induced by qubit 1 is transmitted to qubit 2. As shown here, the two three-junction qubits experience $\sigma_z \otimes \sigma_z$-type coupling. The flux values have to be adjusted for the influence of circulating currents.

some decohering influences here. All quasiparticle states in the superconductor have to remain unoccupied. In equilibrium, the number is far below 1 at temperatures below 30 mK. Extreme care must be taken to shield the sample from photons. Even 4 K blackbody photons have enough energy to break a Cooper pair. Adequate shielding is possible on the time scale of our computer. Inductive coupling to bodies of normal metal has to be avoided. By decoupling the qubit from electrical potentials, we have eliminated coupling to charged defects in substrate or tunnel barriers. The aluminum nuclei have a spin that is not polarized by the small magnetic fields at our temperature of 25 mK. Statistical fluctuations will occur, but their time constant is very long because of the absence of electronic quasi-particles. The net effect will be a small static offset of the level splitting, within the scale of the variations due to fabrication. The dephasing time that results from unintended dipole-dipole coupling of qubits is longer than 1 ms if the qubits are farther apart than 1 μm. Emission of photons is negligible for the small loop. Overall, the sources of decoherence that we know allow for a decoherence time above 1 ms.

Requirements for a quantum computer are that the qubits can be prepared in well-defined states before the start of the computation and that their states can be measured at the end. Initialization will proceed by cooling the computer to below 50 mK and having the qubits settle in the ground state. For the measurement, a generated flux of $10^{-3}\Phi_o$ in an individual qubit can be detected with a SQUID if enough measuring time is available. A good SQUID has a sensitivity of 10 $^{-5}\Phi_o/\mathrm{Hz}^{1/2}$, so that a time of 100 μs is required. Usual SQUIDs have junctions that are shunted with normal metal. The shunt introduces severe decoherence in a qubit when the SQUID is in place, even if no measurement is performed. We are developing a nonshunted SQUID that detects its critical current by discontinuous switching. For a measurement at the end of a quantum computation scheme, the qubit can be frozen by an adiabatic increase of the tunnel barrier between the two qubit states. As Fig. 2 indicates, we can increase the barrier by a change of control current. A similar procedure, as suggested by Shnirman and Schön (*14*), for charge qubits can be followed.

The proposed qubit should be of considerable interest for fundamental studies of macroscopic quantum coherence, apart from its quantum computing potential. Compared with the radio frequency SQUID systems that have been used in attempts to observe such effects (*16*) and also have been suggested as possible qubits for quantum computation (*17*), the much smaller size of the qubit decouples it substantially better from the environment.

References and Notes

1. S. Lloyd, *Science* **261**, 1569 (1993).
2. C. H. Bennett, *Phys. Today* **48** (no. 10), 24 (1995); D. P. DiVincenzo, *Science* **270**, 255 (1995); T. P. Spiller, *Proc. IEEE* **84**, 1719 (1996).
3. S. Lloyd, *Sci. Am.* **273** (no. 4), 140 (1995).
4. Q. A. Turchette, C. J. Hood, W. Lange, H. Mabuchi, H. J. Kimble, *Phys. Rev. Lett.* **75**, 4710 (1995).
5. C. Monroe, D. M. Meekhof, B. E. King, W. M. Itano, D. J. Wineland, *ibid.*, p. 4714.
6. N. A. Gershenfeld and I. L. Chuang, *Science* **275**, 350 (1997).
7. B. Kane, *Nature* **393**, 133 (1998).
8. D. Loss and D. DiVincenzo, *Phys. Rev. A* **57**, 120 (1998).
9. L. B. Ioffe, V. B. Geshkenbein, M. V. Feigel'man, A. L. Fauchère, G. Blatter, *Nature* **398**, 679 (1999).
10. D. V. Averin and K. K. Likharev, in *Mesoscopic Phenomena in Solids*, B. L. Altshuler, P. A. Lee, R. A. Webb, Eds. (North Holland, Amsterdam, 1991), pp. 173–271.
11. W. J. Elion, M. Matters, U. Geigenmuller, J. E. Mooij, *Nature* **371**, 594 (1994); L. S. Kuzmin and D. B. Haviland, *Phys. Rev. Lett.* **67**, 2890 (1991); P. Joyez, D. Esteve, M. H. Devoret, *ibid.* **80**, 1956 (1998).
12. Y. Nakamura, Yu. A. Pashkin, J. S. Tsai, *Nature* **398**, 786 (1999).
13. A. Shnirman, G. Schön, Z. Hermon, *Phys. Rev. Lett.* **79**, 2371 (1997); D. V. Averin, *Solid State Commun.* **105**, 659 (1998); Yu. Makhlin, G. Schön, A. Shnirman, *Nature* **398**, 305 (1999).
14. A. Shnirman and G. Schön, *Phys. Rev. B* **57**, 15400 (1998).
15. T. P. Orlando *et al.*, in preparation.
16. C. D. Tesche, *Phys. Rev. Lett.* **64**, 2358 (1990); R. Rouse, S. Han, J. E. Lukens, *ibid.* **75**, 1614 (1995).
17. M. F. Bocko, A. M. Herr, M. J. Feldman, *IEEE Trans. Appl. Supercond.* **7**, 3638 (1997).

18. We thank J. J. Mazo, C. J. P. M. Harmans, A. C. Wallast, and H. Tanaka for important discussions. This work is partially supported by Army Research Office grant DAAG55-98-1-0369, Stichting voor Fundamenteel Onderzoek der Materie, NSF Award 67436000IRG, and the New Energy and Industrial Technology Development Organization.

22 April 1999; accepted 7 July 1999

Energetic Iron(VI) Chemistry: The Super-Iron Battery

Stuart Licht,* Baohui Wang, Susanta Ghosh

Higher capacity batteries based on an unusual stabilized iron(VI) chemistry are presented. The storage capacities of alkaline and metal hydride batteries are largely cathode limited, and both use a potassium hydroxide electrolyte. The new batteries are compatible with the alkaline and metal hydride battery anodes but have higher cathode capacity and are based on available, benign materials. Iron(VI/III) cathodes can use low-solubility K_2FeO_4 and $BaFeO_4$ salts with respective capacities of 406 and 313 milliampere-hours per gram. Super-iron batteries have a 50 percent energy advantage compared to conventional alkaline batteries. A cell with an iron(VI) cathode and a metal hydride anode is significantly (75 percent) rechargeable.

Improved batteries are needed for various applications such as consumer electronics, communications devices, medical implants, and transportation needs. The search for higher capacity electrochemical storage has focused on a wide range of materials, such as carbonaceous materials (*1*), tin oxide (*2*), grouped electrocatalysts (*3*), or macroporous minerals (*4*). Of growing importance are rechargeable (secondary) batteries such as metal hydride (MH) batteries (*5*), which this year have increased the commercial electric car range to 250 km per charge. In consumer electronics, primary, rather than secondary, batteries dominate. Capacity, power, cost, and safety factors have led to the annual global use of approximately 6×10^{10} alkaline or dry batteries, which use electrochemical storage based on a Zn anode, an aqueous electrolyte, and a MnO_2 cathode, and which constitute the vast majority of consumer batteries. Despite the need for safe, inexpensive, higher capacity electrical storage, the aqueous MnO_2/Zn battery has been a dominant primary battery chemistry for over a century. Contemporary alkaline and MH batteries have two common features: Their storage capacity is largely cathode limited and both use a KOH electrolyte.

We report a new class of batteries, referred to as super-iron batteries, which contain a cathode that uses a common material (Fe) but in an unusual (greater than 3) valence state. Although they contain the same Zn anode and electrolyte as conventional alkaline batteries, the super-iron batteries provide >50% more energy capacity. In addition, the Fe(VI) chemistry is rechargeable, is based on abundant starting materials, has a relatively environmentally benign discharge product, and appears to be compatible with the anode of either the primary alkaline or secondary MH batteries.

The fundamentals of MnO_2 chemistry continue to be of widespread interest (*6*). The storage capacity of the aqueous MnO_2/Zn

Department of Chemistry and Institute of Catalysis Science, Technion—Israel Institute of Technology, Haifa 32000, Israel.

*To whom correspondence should be addressed. E-mail: chrlicht@techunix.technion.ac.il

Superconducting-gap symmetry study using a/c boundary Josephson junctions in $YBa_2Cu_3O_{7-\delta}$ films

Yoshihiro Ishimaru, Jianguo Wen, Naoki Koshizuka, and Youichi Enomoto
Superconductivity Research Laboratory, International Superconductivity Technology Center, 1-10-13 Shinonome, Koto-ku, Tokyo 135, Japan
(Received 4 November 1996)

We have investigated gap symmetry of high-T_c superconductors using Josephson junctions formed along a boundary of an a-axis-oriented $YBa_2Cu_3O_{7-\delta}$ (YBCO) grain surrounded by c-axis-oriented YBCO grains (a/c boundary). There are two types of a/c boundary junctions; one is the boundary between (001) of a-axis-oriented grains and (100) of c-axis-oriented grains, and the other is the boundary between (001) of a-axis-oriented grains and (110) of c-axis-oriented grains. TEM observation shows clean, sharp, and nearly single-facet interface along the grain boundaries in both types. In the case of the (100)-(001) type a/c boundary junction, typical resistively shunted junction (RSJ)-type I-V curves, Shapiro steps under microwave irradiation, and Fraunhofer-like diffraction pattern of I_c under magnetic field are observed, indicating that the boundary works as a Josephson junction. In the case of the (110)-(001)-type a/c boundary junction, typical RSJ type I-V curves and Shapiro steps under microwave irradiation are also observed. However, the diffraction pattern of I_c under magnetic field has the minimum value at zero magnetic field. This property is analogous to one observed for a corner junction which is formed between Pb and YBCO. These results show that the (110) of YBCO has a phase difference of π and $d_{x^2-y^2}$ superconducting-gap symmetry is in CuO_2 planes of YBCO. But, the (001) of YBCO has no phase difference of π in spite of the existence of d-wave symmetry in YBCO. [S0163-1829(97)05317-4]

INTRODUCTION

In the high-T_c oxide superconductors, the emerging possibility of d-wave symmetry of the pairing state has attracted wide attention because this seems strongly to imply a mechanism different from the phonon mechanism of the conventional BCS superconductors. Furthermore, this mechanism gives the possibility of new superconductors with higher T_c and brings about some evolution for device application. From this viewpoint, many investigations have been done. To observe the symmetry, Wollman *et al.* used de-superconducting quantum interference devices (SQUID's) consisting of $YBa_2Cu_3O_{7-\delta}$ (YBCO) and conventional s-wave superconductor Pb.[1] However, it has been pointed out that experiments using the SQUID are susceptible to some fluctuations caused by residual magnetic field, flux trapping, and geometrical symmetry of the SQUID.

To make symmetry of high-T_c superconductors clearly, several researchers used a single Josephson junction consisting of YBCO and Pb.[2-4] If YBCO has an s-wave symmetry, magnetic-field (B) dependence of critical current (I_c) for the Josephson junction shows the conventional Fraunhofer pattern which has a peak at zero field. On the other hand, if it has a d-wave ($d_{x^2-y^2}$) symmetry, B dependence of I_c (I_c-B) for the Josephson junction including a phase difference of π shows the unconventional pattern which has a dip at zero field. Wollman *et al.* observed I_c-B with a dip at zero field for the Josephson junction named a corner junction consisting of (100) and (010) of a YBCO single crystal and Pb.[4] This was considered as evidence for d-wave ($d_{x^2-y^2}$) symmetry. These corner junction properties were also analyzed theoretically as $d_{x^2-y^2}$ symmetry by Tanaka.[5] On the other hand, Sun *et al.* observed a conventional Fraunhofer pattern which has a peak at zero field for a Josephson junction consisting of (001) of YBCO and Pb.[2] This gave evidence for s-wave symmetry. Consequently, we cannot determine the gap symmetry by these experiments.

There is little information about the atomic order roughness or flatness of the interface between YBCO and Pb. This atomic order roughness or flatness is, however, important to determine the superconducting gap symmetry by using Josephson junction because of strong anisotropy of the crystal structure. Furthermore, there are oxidization and deoxidization reactions between the metal Pb and the oxide YBCO, which may cause ambiguity of the gap symmetry. In addition, measurement temperature is limited by the narrow range below T_c of Pb (7.2 K).

In order to study superconducting-gap symmetry of high-T_c superconductors by using Josephson junctions, we should use a junction with an atomic scale flat interface. Many types of Josephson junctions fabricated by various methods have been studied,[6-9] including Josephson junctions using grain boundaries.[10-14] Among them, Josephson junctions using naturally grown grain boundaries between a-axis- and c-axis-oriented grains in YBCO films (we call them a/c boundaries) are interesting, because the atomic scale flat interfaces of the a/c boundaries can be expected by natural formation. Furthermore, two types of a/c boundary junctions are formed; one is the boundary between (001) of a-axis-oriented grains and (100) of c-axis-oriented grains,[15,16] and the other is the boundary between (001) of a-axis-oriented grains and (110) of c-axis-oriented grains.[17]

In this paper, we report microscopic grain-boundary structures and some basic electrical properties for the two types of a/c boundary junctions of YBCO. Especially, the most interesting point in this work is that important information on

superconducting-gap symmetry in YBCO can be obtained by comparing the properties between the two types of a/c boundary junctions.

EXPERIMENT

c-axis-oriented YBCO films including a few a-axis-oriented needlelike grains were fabricated on MgO(001) substrates by pulsed laser deposition. A KrF laser (emission wavelength 248 nm) with power density of about 2 J/cm^2 on stoichiometric high-density targets and the repetition rate of 5 Hz were used as sources. Films of about 200 nm in thickness were grown in oxygen pressure of 200 mTorr at substrate temperature of 780 °C. These conditions are almost the same as those for perfect x-axis-oriented films except for defective substrates. We used the MgO substrate without any annealing treatment to get high-quality films. It is well known that a-axis-oriented grains of YBCO films are fabricated by decreasing the growth temperature, following inferior crystallinity and superconducting properties.[18] In this work, however, we can get the a-axis-oriented needlelike grains in the c-axis-oriented films without decreasing the growth temperature and particular post annealing.

Structures of the films were appraised by x-ray diffraction (XRD) and atomic force microscopy (AFM). Transmission electron microscopy (TEM) samples were prepared for both planar and cross-sectional views to obtain a whole image of a needlelike grain. Electric properties of the grain boundary were observed by a constricted electrode across the boundary. The constricted line with a length of 30 μm and a width of 5 μm were fabricated by photolithography and the Ar-ion-milling technique. In addition, the focused Ga ion-beam (FIB) technique was sometimes used to fabricate the pattern including only one a-axis-oriented grain in the constricted line. I-V characteristics were measured by the usual four-probe method under microwave and magnetic field from 4.2 K to T_c. Magnetic field was applied perpendicular to the film surface by a solenoid coil.

EXPERIMENTAL RESULTS

Microstructure

In our films, grains with a needlelike shape were observed from a topview of thin films. Figure 1(a) shows an optical microscopy surface image of our sample for I-V measurement. The needlelike grains have a length of 5–20 μm and a width of about 200 nm. Most of the direction of the long side is parallel to [100] or [010] of the MgO substrate. There are a few needlelike grains whose direction of the long side is parallel to [110] of the MgO substrate. Figure 1(b) shows an optical microscope surface image of the sample with [110]-type needlelike grains. From the AFM image, the needlelike grains stuck out of the planar parts of the films as pointed protrusion to a height of 100 nm above the surface.

The XRD pattern of the film shown in Fig. 2 consists of only two kinds of diffraction peaks: strong peaks ($00l$) from the c-axis-oriented grains and weak ones ($m00$) from the a-axis-oriented grains. No observation of other diffraction peaks except for the MgO substrate means that most of the needlelike grains are of the a-axis orientation in the entire film.

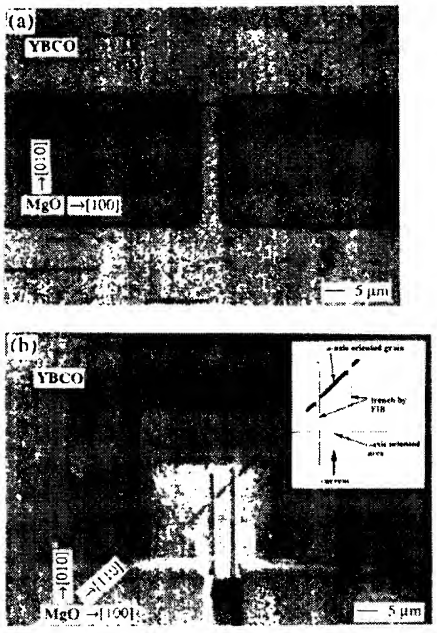

FIG. 1. Micrograph image of the (100)-(001)-type a/c boundary junction (a), and the (110)-(001)-type a/c boundary junction (b). Bridge size with length of 30 μm and width of 5 μm. The inset of (b) is a schematic illustration of the sample which was fabricated by focused-ion-beam (FIB) technique

Figure 3 shows plane-view and cross-sectional lattice images of a needlelike grain being parallel to [100] or [010] of the MgO substrate by TEM. These images show that the needlelike grain is an a-axis-oriented single crystal and has tabular habit vertical to the substrate. Their dominant epitaxial relationship with respect to the c-axis-oriented regions is [100] a-axis-oriented grain ∥[001] c-axis-oriented grain, and [001] a-axis-oriented grain ∥[100] c-axis-oriented grain. Consequently, the interface structure of the boundaries are formed with (100) and (001) YBCO surfaces. We call this type of grain boundary the (100)-(001)-type a/c boundary. There is a little lattice mismatch between these directions, but TEM revealed well defined, straight grain boundaries without any dislocations and any particulates. This clean in-

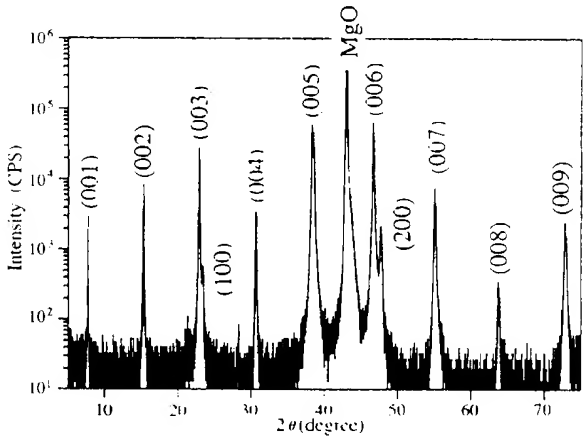

FIG. 2. XRD diffraction pattern of the film.

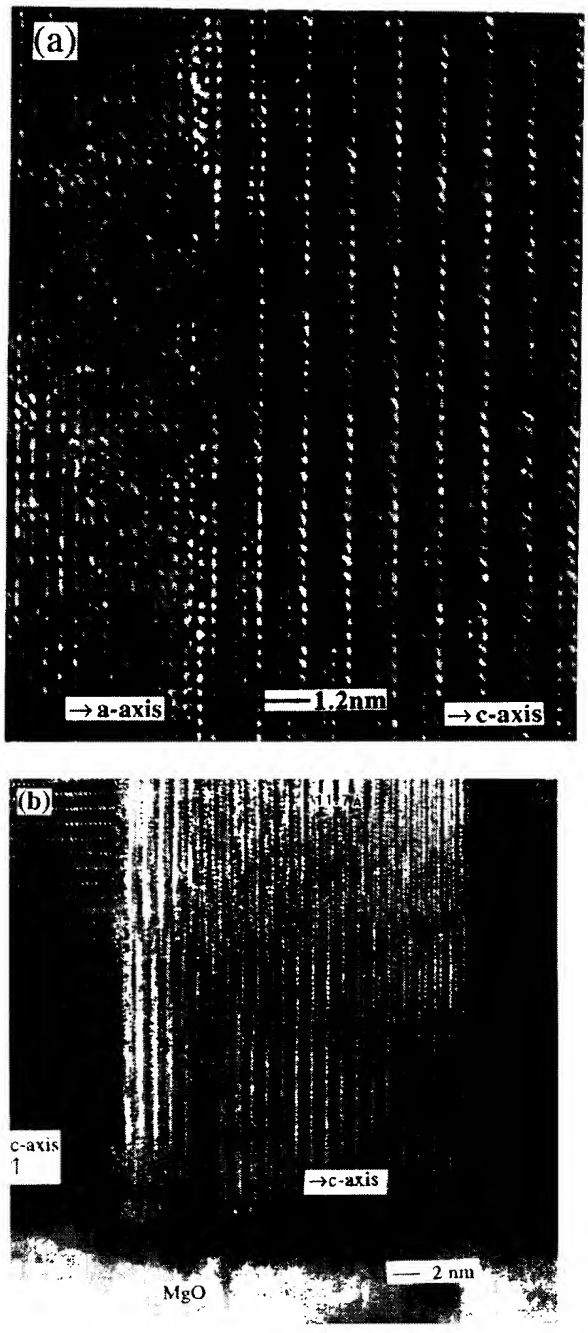

FIG. 3. Plane-view (a) and cross-sectional (b) TEM images of the (100)-(001)-type a/c boundary between a-axis- and c-axis-oriented YBCO grains.

terface is different from the a/c boundary fabricated on an artificially modulated substrate, in which there is some roughness on a microscopic scale.[13] The cross-sectional TEM image of Fig. 3(b) shows that the a-axis-oriented grain grows over the surface of films from about 1 nm thick amorphous layer on the substrates. Consequently, this structure indicates that the superconductive current must flow through this grain because the amorphous layer is not superconducting.

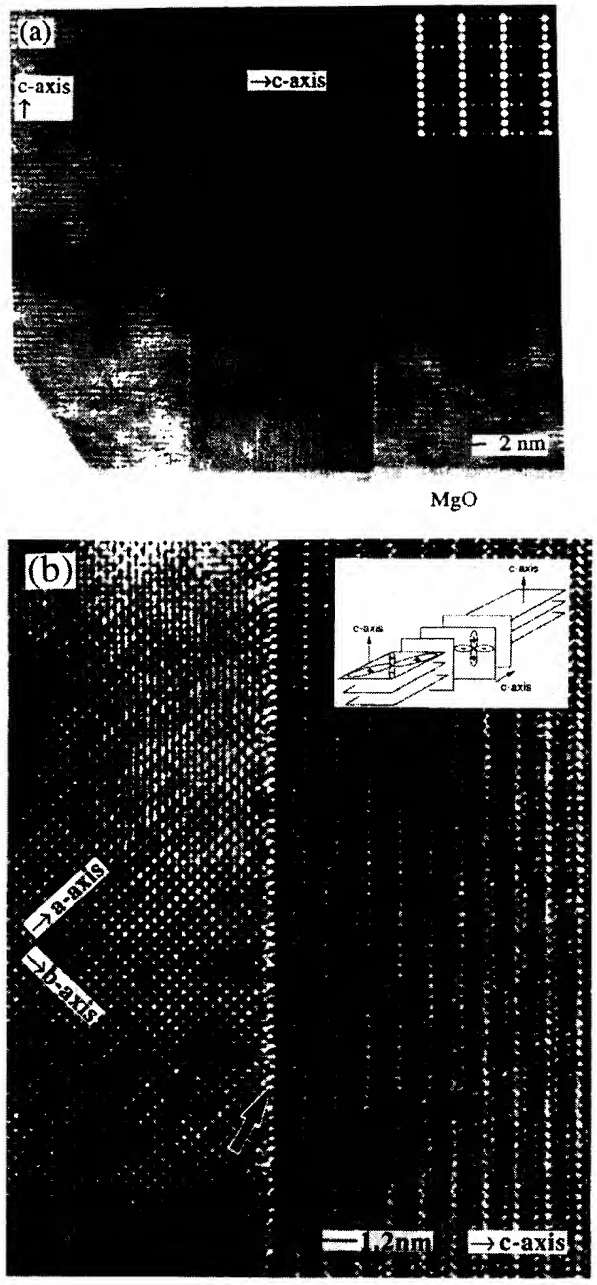

FIG. 4. Cross-sectional (a) and plane-view (b) TEM images of the (110)-(001)-type a/c boundary between a-axis- and c-axis-oriented YBCO grains. The inset in (a) is the electron-diffraction pattern which comes from both grains. The inset (b) is the schematic structure of these grains. The arrow in (b) shows the grain boundary between (001) of the a-axis-oriented grain and (110) of the c-axis-oriented grain.

Figure 4 shows plane-view and cross-sectional lattice images of a needlelike grain being parallel to [110] of the MgO substrate by TEM. The grain is also an a-axis-oriented single crystal. The cross-sectional image shows that the needlelike grains grow right on the substrate. These microstructures are the same as in the [100]-type needlelike grains except for their directions. Their dominant epitaxial relationship with

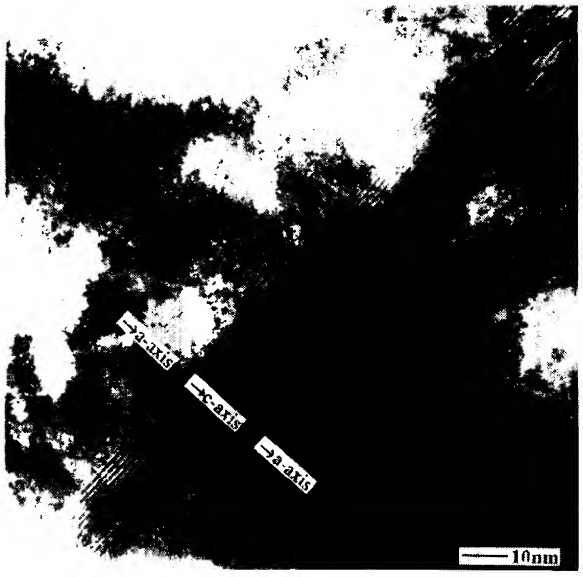

FIG. 5. Wider plane-view TEM image of the (100)-(001)-type a/c boundary between a-axis- and c-axis-oriented YBCO grains.

respect to the c-axis and a-axis-oriented regions is a [100] a-axis-oriented grain ∥[001] c-axis-oriented grain, and a [001] a-axis-oriented grain ∥[110] c-axis-oriented grain. This epitaxial relationship is also confirmed from the electron-diffraction pattern in Fig. 4(a) which comes from both of the grains. Consequently, the interface structure of the boundaries formed with (110) and (001) YBCO surfaces. We call this type of grain boundary the (110)-(001)-type a/c boundary. The interface structure of the boundaries is 90° basal-plane-faced tilt boundary in addition to 45° rotation about the [001] in the c-axis-oriented area. The schematic structure of these grains is shown in the inset of Fig. 4(b). In the plane-view image, there is a large lattice mismatch ($1-\sqrt{2}$) between (100) or (010) in the a-axis grain and (110) in the c-axis grain along the boundary. This interface, however, shows a rather clean microstructure without large size dislocation. But the distortion due to the mismatch is only localized in one or two atomic layers at the interface. This type of a-axis-oriented grain growth is supported by a MgO substrate on which 45° tilt grains are observed sometimes.[19]

These two types of a/c boundary junctions are the most suitable for studying superconducting wave-function symmetry by Josephson junction, because they have atomic scale flat interfaces shown by TEM. Figures 3 and 4 only show local area structures, but actually a wider area also shows the same sharp interface shown by a plane-view TEM image in Fig. 5. Even in a wide range image of the (100)-(001)-type a/c boundary, an atomic scale flat interface is realized.

Plane-view TEM observation also shows that there are twin boundaries in c-axis-oriented films for both types. Therefore, on an a/c boundary junction structure, an a-axis-oriented needlelike grain is across these twin boundaries in c-axis-oriented film. However, there are no twin boundaries in a-axis-oriented needlelike grains for both types. This is because, grain boundaries by twins have never been observed in plane-view or cross-sectional TEM images of needlelike grains.

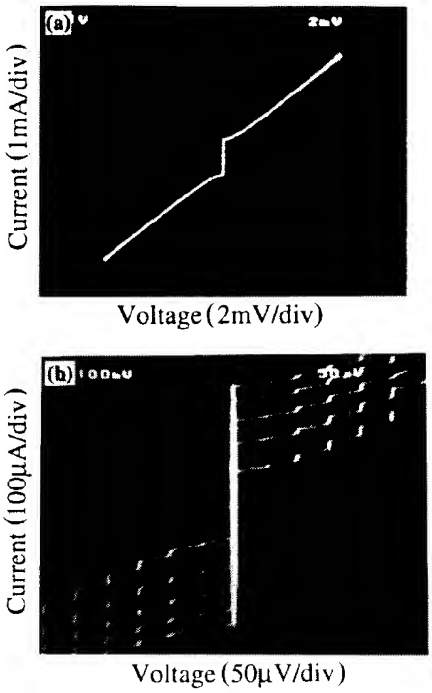

FIG. 6. I-V characteristics of the (100)-(001)-type a/c boundary junction at 28 K (a), and I-V characteristics under 19.49 GHz microwave irradiation of different power at 4.2 K (b).

Finally, we mention why atomic scale flat interfaces are formed along the a/c boundaries. An a-axis-oriented grain grows preferentially along a line-type microstep. Actually, the TEM image in Fig. 3(b) shows existence of a small step of MgO at the bottom edge of the a-axis-oriented grain. After the a-axis-oriented seed layer is formed, the a-axis-oriented grain grows epitaxially on it. In addition, the higher growth rate of the a axis than the c axis makes the a-axis-oriented grains stick out of the c-axis-oriented plain surface. Consequently, the c-axis-oriented films start or stop growing at both walls of the a-axis-oriented grain and surround it. Thus, the atomic scale flat interface perpendicular to the substrate is formed even if mismatch is large. However, we should mention the occurrence of a stacking fault in the a-axis-oriented needlelike grain, although it is not observed in our cross-sectional TEM images. According to this model, a-axis grains start to grow from both sides of line-type microgrooves on the substrates. In this case, the stacking fault is generated at the center of the grain and may work as a Josephson junction. This type of stacking fault was actually observed in a-axis-oriented needlelike grains and reported by other researchers[20] as well as in the plane-view images.[28]

I-V characteristics

The T_c of an electrode including the (100)-(001)-type a/c boundary is about 80 K. This value is not so low for a-axis-oriented films. This rather high T_c is caused by the growth temperature of 780 °C which is higher than conventional growth temperature below 700 °C for a-axis-oriented YBCO films.[21] Figure 6(a) shows an I-V curve at 28 K for

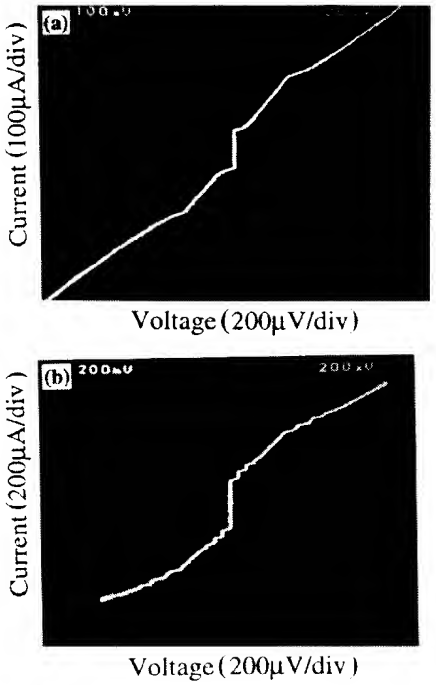

FIG. 7. I-V characteristics of the (110)-(001)-type a/c boundary junction at 4.2 K (a) and I-V characteristics under 19.68 GHz microwave irradiation on the (110)-(001)-type a/c boundary junction at 4.2 K (b).

the (100)-(001)-type a/c boundary formed through only one needlelike grain as shown in Fig. 1(a). Typical resistively shunted-junction (RSJ) characteristics are observed. The value of J_c is 4.4 10^4 A/cm^2 at 4.2 K. Through the current path, two kinds of Josephson junctions can be formed: two Josephson junctions correspond to a/c boundaries, and many Josephson junctions related to intrinsic interlayer between CuO_2 planes in the a-axis-oriented grain. The observed J_c value of 4.4 10^4 A/cm^2 is about two orders smaller than the value 3–5 10^6 A/cm^2 obtained for an a-axis-oriented YBCO film at 4.2 K.[18,21] This result means that the observed weak-link characteristics describe the properties at the interface between a-axis- and c-axis-oriented grains, but not the interplane of the CuO_2 planes. There should be a bend in the I-V curve, if both side junctions of the grain have different critical current. Therefore, no bend in Fig. 6(a) indicates that two a/c boundary Josephson junctions have the same I_c, which is plausible due to the same structure on atomic scale.

Figure 6(b) shows Shapiro steps in I-V curves of the (100)-(001)-type a/c boundary junction under various microwave powers of 19.49 GHz at 4.2 K. These clear Shapiro steps show the (100)-(001)-type a/c boundary works a role of the Josephson junction. I_cR_n product is estimated to be 1.37 mV from the microwave power dependence of Shapiro-step height using the current source model.[22] This value is almost the same as one of the high-quality in-plane rotated grain-boundary junctions reported and satisfies the empirical relation between J_c and I_cR_n.[23] Our junction consists of an a-axis-oriented grain with short coherent length perpendicular to the face of the boundary. Therefore, the rather high I_cR_n value means clear interface along the a/c boundary as

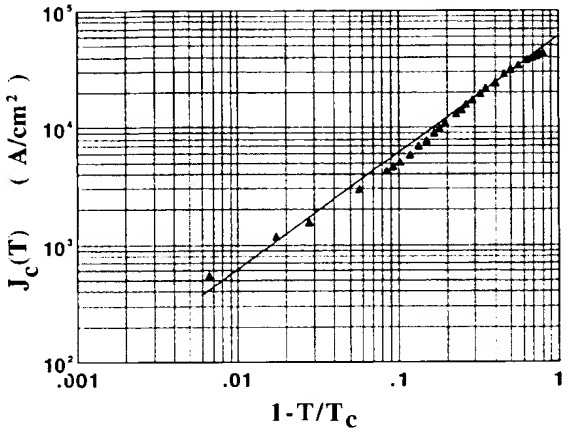

FIG. 8. Temperature dependence of J_c on the (100)-(001)-type a/c boundary junction which is plotted J_c vs (1 T/T_c). The line means that index of the bracket equals 1.

well as TEM observation. From this I_cR_n and I_c of 560 μA, R_n is calculated to be 2.44 Ω at 4.2 K. This value agrees with R_n of 2.41 Ω obtained by extrapolation to high bias voltage in the I-V curve.

Figure 7(a) shows an I-V curve at 4.2 K for the (100)-(001)-type a/c boundary formed through only one needlelike grain as shown in Fig. 1(b). Current flows through the a-axis grain according to a path limited by two drains which were etched by FIB. There is a bend in the I-V curve, which means that two Josephson junctions with different critical currents, I_c's are formed through the current path. These junctions exist in series and closely to each other in a constricted electrode pattern as shown in Fig. 1(b). Both the junctions exhibit typical RSJ-type characteristics. Figure 7(b) shows Shapiro steps in the I-V curves of the (110)-(001)-type a/c boundary junction under microwave of 19.68 GHz at 4.2 K. Two groups of Shapiro steps are observed corresponding to each junction. This result indicates that both junctions play the role of the Josephson junction. As mentioned already, there are two boundaries along both the sides of the a-axis-oriented grain. Therefore, the two junctions observed in the I-V curve are expected to correspond to these grain boundaries. But its probability is low because of different magnetic-field dependence of I_c described later. From the microwave power dependence of the height of Shapiro steps, normal resistance of the junction, R_n, is estimated to be about 2Ω for the lower I_c junctions. In spite of large lattice mismatch density along the boundary, this value of R_n is as low as one of the (100)-(001)-type a/c boundary junction. This means that resistivity along the boundary is independent of misfit density.

Figure 8 shows a critical current density (J_c) of the (100)-(001)-type a/c boundary junction as a function of temperature. J_c can be observed from 4.2 K to about 80 K which is T_c of the samples. Near T_c, the behavior of J_c can be fit by the functional form $J_c \propto (1 \quad T/T_c)$. Generally, the index of the bracket near 1 means formation of the SIS-type junction, which exhibits hysteresis in an I-V curve.[24] In fact, hysteresis I-V curves were reported for some a/c boundary Josephson junctions.[15] For our sample, no hysteresis structure has been observed yet. A similar inconsistent relation be-

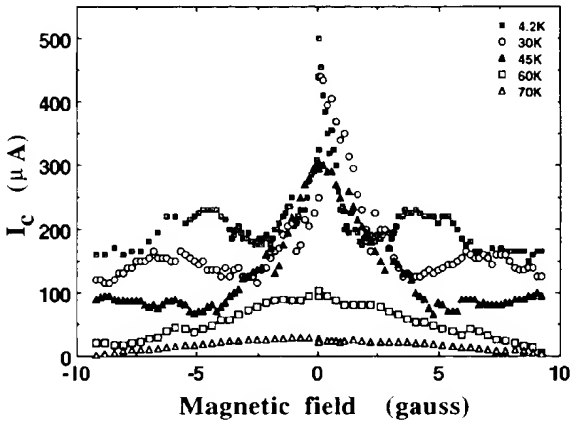

FIG. 9. Magnetic-field dependence of I_c on the (100)-(001)-type a/c boundary junction at various temperatures.

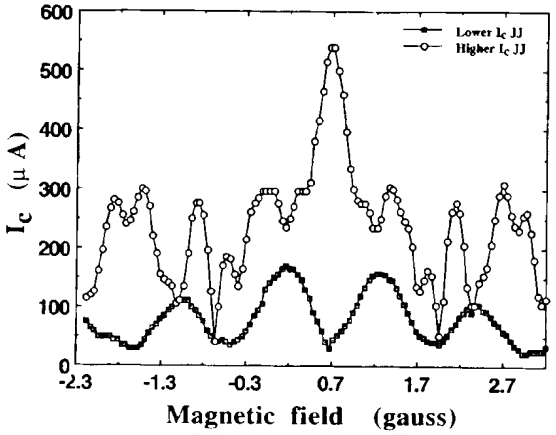

FIG. 10. Magnetic-field dependence of I_c on the (110)-(001)-type a/c boundary junction at 18 K. Minimum I_c value in lower I_c junction occurred at zero magnetic field. This magnetic-field dependence of I_c is analogous to one observed for the s-wave–d-wave corner junction consisted with YBCO and Pb.

tween the index and weak-link properties is observed in other experiments.[25,26] Therefore, the correspondence will have to be clear.

Magnetic-field dependence of I_c

Figure 9 shows the magnetic-field dependence of I_c (I_c-B) for the (100)-(001)-type a/c boundary at various temperatures. In order to obtain information on the lateral uniformity of a junction, the magnetic field was applied normal to a substrate. Magnetic interference patterns are observed below T_c. However, the shapes of the diffraction patterns are quite complicated. At low temperature, the oscillations are nearly triangular which are characteristic of long junction behavior.[27] As the temperature rises, the critical current drops and the oscillations become round and wide. The important point for discussing the symmetry of the superconducting gap is that the I_c-B pattern of the (100)-(001)-type a/c boundary junction has a peak at zero magnetic field.

For the (110)-(001)-type a/c boundary, two junctions with different I_c's are observed in Fig. 7(a) and these I_c's sometimes cross each other during changing magnetic field. Therefore, we carefully obtained I_c's from the entire I-V curves to prevent confusion. Figure 10 shows I_c-B patterns for these two junctions. For the junction with higher I_c, a clear symmetric pattern with a center maximum at about 0.7 G and clear side lobes were observed. This pattern looks like a conventional Josephson junction, for which the I_c peak occurs at real zero magnetic field. Therefore, we think there was a residual magnetic field of 0.7 G at the junction area which comes from terrestrial and external magnetism. The pattern for lower-I_c junction is also symmetric, but it has the minimum value at about 0.7 G magnetic field. Assuming that both the junctions with higher-I_c and lower-I_c are under the same magnetic field due to the close position, minimum I_c value occurs at zero magnetic field. This magnetic-field dependence of I_c is analogous to the one observed for the s-wave–d-wave corner junction reported by Wollman *et al.*[4]

In the case of our sample of the (110)-(001)-type a/c boundary, there are three grain-boundary Josephson junctions through the current path; two junctions are formed along two a/c boundaries and one corresponds to the boundary of the stacking fault as mentioned previously. This situation is shown in Fig. 11. In this situation, two a/c boundary Josephson junctions have the same I-V characteristics because these two boundaries are composed of the same structure in atomic scale, and two a/c boundary Josephson junctions behave like only one Josephson junction in I-V characteristics. Thus, two kinds of I_c-B patterns are observed in I-V characteristics; one corresponds to two a/c boundaries behaving like only one junction and the other corresponds to the stacking fault.

In Fig. 12, one set of the higher and lower I_c patterns is observed at low temperature, and another set of the patterns is observed after heating up to room temperature. This unchanging symmetry of the patterns shows that the diffraction pattern with a dip at zero magnetic field is not caused by the flux trapping generated irregularly.

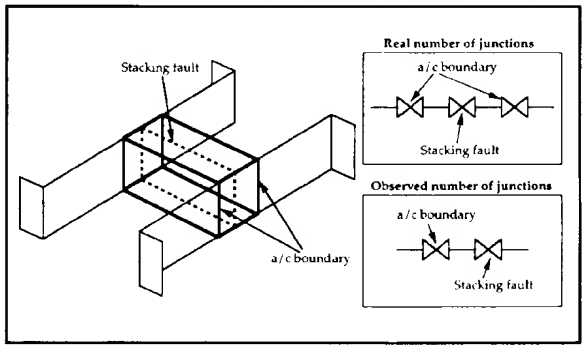

FIG. 11. Schematic structure for our sample of the (110)-(001)-type a/c boundary. There are three grain boundaries through the current path; two junctions are formed along two a/c boundaries and one corresponds to the stacking fault. Two a/c boundary Josephson junctions have the same I-V characteristics because these two boundaries are composed of the same structure in atomic scale, and two a/c boundary Josephson junctions behave like only one Josephson junction in I-V characteristics.

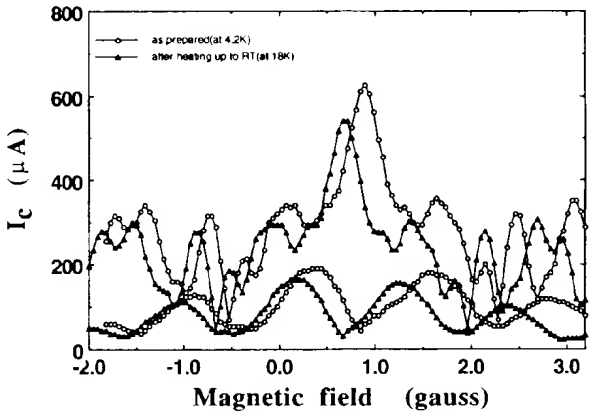

FIG. 12. Temperature dependence of the magnetic-field dependence of I_c patterns with peak and dip at zero magnetic field at different temperature on the (110)-(001)-type a/c boundary junction. As prepared (1), after heating up to room temperature (2).

We have observed I_c-B with the dip at zero magnetic field for another (110)-(001)-type a/c boundary junction. On the other hand, this type of I_c-B pattern has never been observed in the junctions using the (100)-(001)-type a/c boundary. Therefore, we believe this pattern of lower I_c junction is caused along the grain boundary between (110) of the c-axis-oriented grain and (001) of the a-axis-oriented grain. As a result, the higher-I_c junction is formed along a stacking fault in the a-axis-oriented grain.

Figure 13 shows I_c-B patterns for the junction with lower I_c at 4.2, 18, and 36 K. Maximum I_c values decrease with increasing temperature, but symmetry of the patterns is the same. At 36 K, the I_c value at zero magnetic field is suppressed to almost zero.

Figure 14 shows the temperature dependence of I_c for both the (100)-(001) and the (110)-(001) types of a/c boundary Josephson junctions. These two I_c's decrease monotonously with increasing temperature, but they have different temperature dependence. Maximum J_c values at 4.2 K of the (110)-(001)-type a/c boundary junction was 1.4 10^4 A/cm^2. This J_c value is about 1/3 smaller than 4.4 10^4

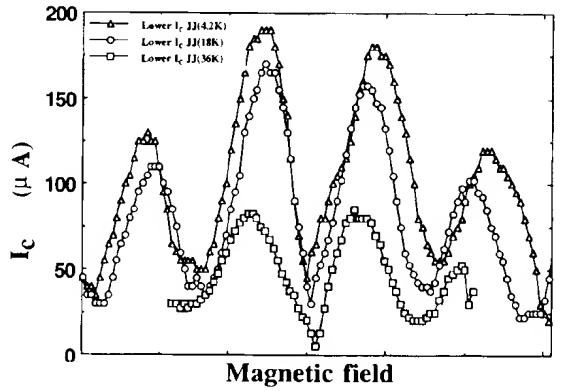

FIG. 13. Temperature dependence of the magnetic-field dependence of I_c patterns at 4.2, 18, and 36 K on the (110)-(001)-type a/c boundary junction with minimum I_c value at zero magnetic field.

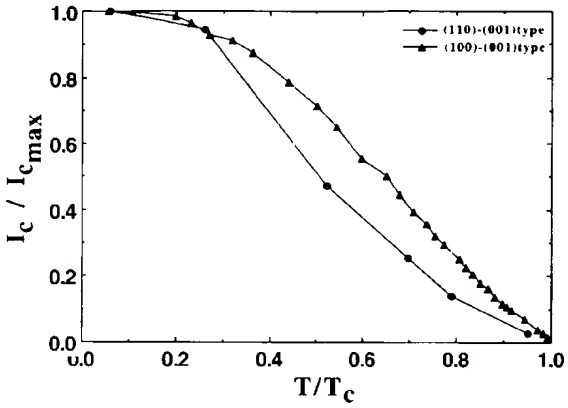

FIG. 14. Temperature dependence of I_c at the (100)-(001)- and the (110)-(001)-type a/c boundary junctions.

A/cm^2 of the (100)-(001)-type a/c boundary junction. This small J_c and different temperature dependence of I_c may be related to the structure difference between the boundaries as well as superconducting-gap symmetry in YBCO.

DISCUSSION

From TEM images, it is clear that the two types of a/c boundary junctions used in this experiment have atomic scale flatness and clear interfaces of the boundaries. In addition, atomic species along both types of the boundaries were determined. BaO layers are terminated at the (001) for both types of a/c boundary.[28] Thus, superconducting-gap symmetry is held at these clear interfaces. We would like to mention again the important role of the flat and clear interface. There are some experiments using grain-boundary Josephson junctions for the superconducting-gap symmetry.[29–31] But, microscale inhomogeneity exists along these grain boundaries fabricated by bicrystal (including tricrystal) and biepitaxial methods,[32,33] and smears I_c-B pattern.

The I_c-B pattern with a dip at zero field has been observed in junctions using the (110)-(001)-type a/c boundary, but never in the (100)-(001)-type a/c boundary. Here, we discuss the size effect on Josephson junctions. A theoretical analysis reports that magnetic-field dependence of I_c should show a peak at zero field for a long Josephson junction even with phase difference of π.[34] Therefore, the I_c-B pattern with a peak at zero field does not mean direct evidence of the s-wave junction. In our experiments, some diffraction patterns were observed with long or small junction behavior for the (100)-(001) a/c boundary junctions by changing temperature and pattern width. But, all of these diffraction patterns show the I_c-B pattern with a peak at zero field. Therefore, we believe that the peak at zero field in the I_c-B pattern is an intrinsic property of the (100)-(001)-type a/c boundary.

In order to discuss superconducting-gap symmetry in YBCO, we summarize our experimental results in Table I, together with the results reported before. The dip at zero field in the I_c-B pattern suggests that the phase difference of π occurs at the boundary of the junction, which is called a π junction. And, if a d-wave symmetry gap is in YBCO, phase difference appears along the points on the face [e.g., (100),

TABLE I. Existence of dip at zero field in I_c-B pattern for various couples of Josephson junctions.

Couple	Existence of dip at zero field in I_c-B pattern
(100)-(001) YBCO	No
(110)-(001) YBCO	Yes
Pb-(001) YBCO	No
Pb-(100) YBCO	No
Pb-corner YBCO	Yes

(110), (001) face]. Junctions consisting of Pb and YBCO edges of the (100) or (010) face have conventional I_c-B patterns.[4,35] This suggests that there is no phase difference of π at the (100) or (010) faces of YBCO, because Pb is an s-wave superconductor. By the way, the (100)-(001)-type a/c boundary junctions have no dip in I_c-B patterns. Therefore, there is also no phase difference of π at (001) of YBCO. This lack of phase difference at (001) is consistent with the experimental results of the Josephson junction consisting of Pb and (001) YBCO which Sun and co-workers reported.[2,36] On the other hand, the I_c-B pattern of the (110)-(001) a/c boundary junction behaves similarly to the π junction which consists of Pb and a corner of the YBCO single crystal.[4,35] This coincidence strongly suggests that there is a phase difference of π at (110),[37] and the $d_{x^2-y^2}$ superconducting-gap symmetry in ab planes of YBCO. Thus, the following two points about the phase for some planes of YBCO are clear.

(1) (001) of YBCO has no phase difference of π.

(2) (110) of YBCO has phase difference of π. This is consistent with the $d_{x^2-y^2}$ superconducting-gap symmetry being in the ab planes of YBCO.

Next, we discuss why the Josephson tunneling along the c direction of YBCO has no phase difference of π under the situation in which the $d_{x^2-y^2}$ superconducting-gap symmetry is in the ab planes of YBCO. It is easier to think that (001) of YBCO is expected to have phase difference of π which occurs by total cancellation of the phase at (001) due to a $d_{x^2-y^2}$ symmetry gap. But actually, our experimental results on the a/c boundary Josephson junctions suggest that the (001) of YBCO has no phase difference of π. This interpretation can explain many experimental results using Josephson junctions with YBCO (edge and corner junctions between YBCO and Pb, junction between Pb and (001) of YBCO, two types of the a/c boundary junctions). Therefore, the mechanism that we need must explain two points about the phase relation mentioned above. In addition, the difference of temperature dependence of I_c between the (100)-(001) and the (110)-(001) a/c boundary must be explained by a theory of the superconducting mechanism. Recently, many researchers have been interested in the Josephson-junction properties along the c direction or gap symmetry of the (001) of YBCO, and some research with theoretical analysis has been reported.[38-41]

CONCLUSION

Two types of a/c Josephson junctions were formed along a boundary of an a-axis-oriented grain surrounded by c-axis-oriented grains of $YBa_2Cu_3O_{7-\delta}$. One has been fabricated along boundaries between (001) of a-axis-oriented YBCO grains and (100) of c-axis-oriented YBCO grains, and the other has been fabricated along boundaries between (001) of a-axis-oriented YBCO grains and (110) of c-axis-oriented YBCO grains. TEM observation shows clear lattice images along the a/c grain boundaries in both types on atomic scale. In I-V characteristics, Shapiro steps under microwave irradiation and the diffraction patterns of I_c under magnetic field were observed in both types, indicating that these boundaries work as Josephson junctions.

In the case of the (100)-(001)-type a/c boundary junction, the conventional magnetic-field dependence of I_c with a peak at zero magnetic field is observed. In the case of the (110)-(001)-type a/c boundary junction, the diffraction pattern of I_c under magnetic field has the minimum value at zero magnetic field. These results show that the (110) of YBCO has a phase difference of π and $d_{x^2-y^2}$ superconducting-gap symmetry is in CuO_2 planes of YBCO. But, the (001) of YBCO has no phase difference of π in spite of the existence of d-wave symmetry in ab planes of YBCO. Our experimental results for these a/c boundary Josephson junctions are expected to be analyzed theoretically.

ACKNOWLEDGMENTS

We wish to thank K. Hayashi for preparation of thin films. We would like to thank S. Tanaka for his encouragement and T. Usagawa, K. Saitoh, and K. Tanabe for helpful discussions. This work was supported by NEDO for the R&D of Industrial Science and Technology Frontier Program.

[1] D. A. Wollman, D. J. Van Harlingen, W. C. Lee, D. M. Ginsberg, and A. J. Leggett, Phys. Rev. Lett. **71**, 2134 (1993).
[2] A. G. Sun, D. A. Gajewski, M. B. Maple, and R. C. Dynes, Phys. Rev. Lett. **72**, 2267 (1994).
[3] I. Iguchi and Z. Wen, Phys. Rev. B **49**, 12 388 (1994).
[4] D. A. Wollman, D. J. Van Harlingen, J. Giapintzakis, and D. M. Ginsberg, Phys. Rev. Lett. **74**, 797 (1995).
[5] Y. Tanaka, Phys. Rev. Lett. **72**, 3871 (1994).
[6] J. Gao, W. A. Aarnink, G. Gerritsma, and H. Rogalla, Physica C **171**, 126 (1991).
[7] C. T. Rogers, A. Inam, M. S. Hegde, B. Dutta, X. D. Wu, and T. Venkatesan, Appl. Phys. Lett. **55**, 2032 (1989).
[8] Ch. Neumann, K. Yamaguchi, K. Hayashi, K. Suzuki, Y. Enomoto, and S. Tanaka, Physica C **210**, 138 (1993).
[9] M. S. Dilorio, S. Yoshizumi, K.-Y. Yang, J. Zhang, and M. Maung, Appl. Phys. Lett. **58**, 2552 (1991).
[10] D. Dimos, P. Chaudhari, J. Mannhart, and F. K. Legoues, Phys. Rev. Lett. **61**, 219 (1988).
[11] K. Char, S. Colclough, S. M. Garrison, N. Newman, and G. Zaharchuk, Appl. Phys. Lett. **59**, 733 (1991).

[12] C. L. Jia, B. Kabius, K. Urban, K. Herrmann, G. J. Cui, J. Schubert, W. Zanden, A. I. Braginski, and C. Heiden, Physica C **175**, 545 (1991).
[13] D. J. Lew, Y. Suzuki, A. F. Marshall, T. H. Geballe, and M. R. Beasley, Appl. Phys. Lett. **65**, 1584 (1994).
[14] M. Konishi and Y. Enomoto, Jpn. J. Appl. Phys. **34**, L1271 (1995).
[15] B. M. Moeckly and R. A. Buhrman, Appl. Phys. Lett **65**, 3126 (1994).
[16] Y. Ishimaru, K. Hayashi, and Y. Enomoto, Jpn. J. Appl Phys. **34**, L1123 (1995).
[17] Y. Ishimaru, J. G. Wen, K. Hayashi, Y. Enomoto, and N. Koshizuka, Jpn. J. Appl. Phys. **34**, L1532 (1995).
[18] J. F. Hamet, B. Mercey, M. Hervieu, and B. Raveau, Physica C **193**, 465 (1992).
[19] D. H. Shin, J. Silcox, S. E. Russek, D. K. Lathrop, B. Moeckly, and R. A. Buhrman, Appl. Phys. Lett. **57**, 508 (1990).
[20] C. Traeholt, J. G. Wen, V. Svetchnikov, A. Delsing, and H. W. Zandbergen, Physica C **206**, 318 (1993).
[21] S. Mahajan, W. Ito, Y. Yoshida, and T. Morishita, Physica C **213**, 445 (1993).
[22] K. Yamaguchi, K. Suzuki, S. Tanaka, and A. Kawaji, IEICE Trans. C-II, **J77-C-II**, 399 (1994) (in Japanese).
[23] R. Gross, P. Chaudhari, M. Kawasaki, and A. Gupta, Phys. Rev. B **42**, 10 735 (1990).
[24] P. G. De Gennes, *Superconductivity of Metals and Alloys* (Benjamin, New York, 1966).
[25] Y. Fukumoto, S. Hataski, R. Ogawa, and Y. Kawate, Appl. Phys. Lett. **64**, 782 (1994).
[26] H. Suzuki, Y. Fujiwara, Y. Hirotsu, T. Yamashita, and T. Oikawa, Jpn. J. Appl. Phys. **32**, 1601 (1993).
[27] A. Barone and G. Paterno, *Physics and Applications of the Josephson Effect* (Wiley, New York, 1982), Chap. 5.
[28] J. G. Wen, Y. Ishimaru, K. Hayashi, Y. Enomoto, and N. Koshizuka, Mater. Sci. Eng. B **41**, 82 (1996).
[29] J. H. Miller, Jr., Q. Y. Ying, Z. G. Zou, N. Q. Fan, J. H. Xu, M. F. Davis, and J. C. Wolfe, Phys. Rev. Lett. **74**, 2347 (1995).
[30] P. Chaudhari and Shawn-Yu Lin, Phys. Rev. Lett. **72**, 1084 (1994).
[31] J. Mannhart, B. Mayer, and H. Hilgenkamp, Z. Phys. B **101**, 175 (1996); H. Hilgenkamp, J. Mannhart, and B. Mayer, Phys. Rev. B **53**, 14 586 (1996).
[32] C. Traeholt, J. G. Wen, H. W. Zandbergen, Y. Shen, and J. W. M. Hilgenkamp, Physica C **230**, 425 (1994).
[33] C. A. Copetti, F. Ruders, B. Oelze, Ch. Buckal, B. Kabius, and J. W. Seo, Physica C **253**, 63 (1995).
[34] J. H. Xu, J. H. Miller, Jr., and C. S. Ting, J. Supercond. **8**, 649 (1995).
[35] D. A. Brawner and H. R. Ott, Phys. Rev. B **53**, 8249 (1996).
[36] A. G. Sun, A. Truscott, A. S. Katz, R C. Dynes, B. W. Veal, and C. Gu, Phys. Rev. B **54**, 6734 (1996).
[37] Y. Ishimaru, T. Utagawa, and Y. Enomoto (unpublished).
[38] M. Sigrist, K. Kuboki, P. A. Lee, A. J. Millis, and T. M. Rice, Phys. Rev. B **53**, 2835 (1996).
[39] M. B. Walker, Phys. Rev. B **53**, 5835 (1996).
[40] M. B. Walker and J. Leuttmer-Strathmann, Phys. Rev. B **54**, 588 (1996).
[41] K. A. Muller, J. Phys. Soc. Jpn. **65**, 3090 (1996).